# Inhibition of Ephrin B2 Reverse Signaling Abolishes Multiple Myeloma Pathogenesis

Joshua P. Sasine[1,2,3,4], Natalia Y. Kozlova[1,2], Lisa Valicente[1,2], Jennifer Dukov[1,2], Dana H. Tran[1,2], Heather A. Himburg[5], Sanjeev Kumar[4], Sarah Khorsandi[1], Aldi Chan[1], Samantha Grohe[1], Michelle Li[6], Jenny Kan[6], Mary E. Sehl[6], Gary J. Schiller[6], Bryanna Reinhardt[1], Brijesh Kumar Singh[7], Ritchie Ho[7], Peibin Yue[1], Elena B. Pasquale[8], and John P. Chute[1,2,3,4]

## ABSTRACT

Bone marrow vascular endothelial cells (BM EC) regulate multiple myeloma pathogenesis. Identification of the mechanisms underlying this interaction could lead to the development of improved strategies for treating multiple myeloma. Here, we performed a transcriptomic analysis of human ECs with high capacity to promote multiple myeloma growth, revealing overexpression of the receptor tyrosine kinases, EPHB1 and EPHB4, in multiple myeloma–supportive ECs. Expression of ephrin B2 (EFNB2), the binding partner for EPHB1 and EPHB4, was significantly increased in multiple myeloma cells. Silencing EPHB1 or EPHB4 in ECs suppressed multiple myeloma growth in coculture. Similarly, loss of EFNB2 in multiple myeloma cells blocked multiple myeloma proliferation and survival *in vitro*, abrogated multiple myeloma engraftment in immune-deficient mice, and increased multiple myeloma sensitivity to chemotherapy. Administration of an EFNB2-targeted single-chain variable fragment also suppressed multiple myeloma growth *in vivo*. In contrast, overexpression of *EFNB2* in multiple myeloma cells increased STAT5 activation, increased multiple myeloma cell survival and proliferation, and decreased multiple myeloma sensitivity to chemotherapy. Conversely, expression of mutant *EFNB2* lacking reverse signaling capacity in multiple myeloma cells increased multiple myeloma cell death and sensitivity to chemotherapy and abolished multiple myeloma growth *in vivo*. Complementary analysis of multiple myeloma patient data revealed that increased *EFNB2* expression is associated with adverse-risk disease and decreased survival. This study suggests that EFNB2 reverse signaling controls multiple myeloma pathogenesis and can be therapeutically targeted to improve multiple myeloma outcomes.

**Significance:** Ephrin B2 reverse signaling mediated by endothelial cells directly regulates multiple myeloma progression and treatment resistance, which can be overcome through targeted inhibition of ephrin B2 to abolish myeloma.

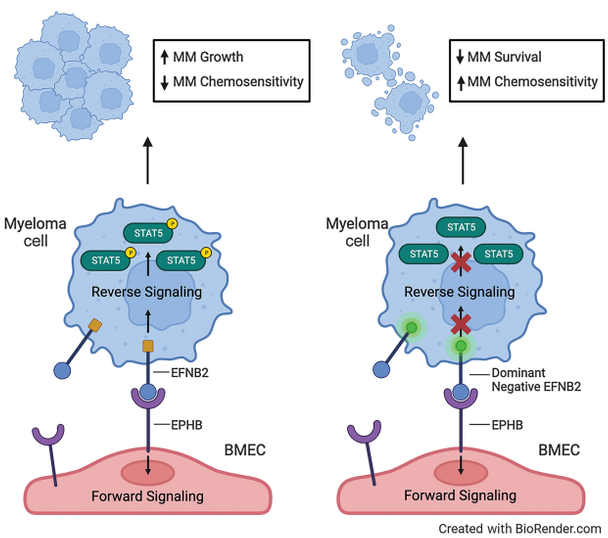


## Introduction

Multiple myeloma is one of the most common hematologic malignancies (1), and although patient survival has increased over the past two decades as a result of modern therapies, multiple myeloma remains an incurable disease (2). Multiple myeloma presents in early stages in the bone marrow (BM) and cells within the BM niche support the pathogenesis of the disease (3–7). For example, BM osteoblasts endow quiescent multiple myeloma cells with colony-forming potential (8, 9) and BM fibroblasts promote multiple myeloma cell growth and survival in the BM (9). Multiple myeloma cells support their own growth and disease progression via production of proangiogenic signals (10–13) and endothelial cells (EC) can support multiple myeloma cell niches within the BM (14). Angiogenic myeloid cells can also drive the pathologic evolution of multiple myeloma via expansion of a multiple myeloma vascular niche (15). Furthermore,

[1]Division of Hematology & Cellular Therapy, Department of Medicine, Cedars-Sinai Medical Center, Los Angeles, California. [2]Cedars-Sinai Samuel Oschin Comprehensive Cancer Institute, Los Angeles, California. [3]Regenerative Medicine Institute, Cedars-Sinai Medical Center, Los Angeles, California. [4]Department of Medicine, Cedars Sinai Medical Center, Los Angeles, California. [5]Department of Radiation Oncology, Medical College of Wisconsin, Milwaukee, Wisconsin. [6]Division of Hematology/Oncology, Department of Medicine, UCLA, Los Angeles, California. [7]Department of Biomedical Sciences, Cedars Sinai Medical Center, Los Angeles, California. [8]Sanford Burnham Prebys Medical Discovery Institute, San Diego, California.

**Corresponding Authors:** Joshua Sasine, Division of Hematology and Cellular Therapy, Cedars-Sinai Medical Center, 8700 Beverly Boulevard, Los Angeles, CA 90048. E-mail: Joshua.sasine@cshs.org; and John P. Chute, Division of Hematology and Cellular Therapy, Cedars-Sinai Medical Center, 8700 Beverly Boulevard, Los Angeles, CA 90048. E-mail: john.chute@cshs.org

Cancer Res 2024;84:919–34

**doi:** 10.1158/0008-5472.CAN-23-1950

immunomodulatory drugs, such as lenalidomide and thalidomide, suppress multiple myeloma growth in patients, at least in part, via antiangiogenic effects (16). However, the precise mechanisms through which BM ECs promote multiple myeloma growth within the niche remain poorly understood.

EPH proteins are transmembrane tyrosine kinase receptors that bind to membrane-anchored ligands, called ephrins, and play an important role in short-distance cell–cell communication during morphogenesis, axon guidance during nervous system development, and vascular development (17–20). Uniquely, EPH–Ephrin complexes can produce bidirectional signaling, thereby affecting the EPH receptor–expressing cell (forward signaling) and the ephrin-expressing cell (reverse signaling), and ephrins can also regulate signals by EPH receptors in the same cell (17). Reverse signaling through ephrin B2 has been shown to regulate diverse organ functions, such as axon synapse formation and chemoattraction (21, 22), pancreatic islet formation (23), and angiogenesis (24). In homeostasis, EPHB4 is expressed by BM ECs and EPHB4 signaling through Ephrin B2 regulates hematopoietic progenitor cell mobilization (25). EPH receptors are also expressed in several human carcinomas (26), and EPH receptor expression has been associated with progression of cancer disease (27). For example, EPHA2 expression has been associated with increased brain metastasis in non–small cell lung cancer (26, 27) and therapy resistance (28). EPHA2 expression also transforms normal breast epithelial cells (29) and promotes HER2 inhibitor resistance (30). Interestingly, expression of the EPH ligand, ephrin B2, has been linked to poor response to chemotherapy, decreased overall survival and disease-free survival in head and neck squamous cell carcinoma, pancreatic and bladder carcinoma (31). Taken together, these studies suggest that EPH–Ephrin signaling may have an important role in regulating the pathogenesis of several human cancers.

Via differential transcriptomic analysis, we discovered that genes encoding EPH receptor tyrosine kinases, EPHB1 and EPHB4, were upregulated in human ECs that support multiple myeloma growth, and that EFNB2, the transmembrane ligand for EPHB1 and EPHB4, is highly expressed by multiple myeloma cells. Targeted inhibition of EFNB2 reverse signaling suppressed multiple myeloma survival and proliferation *in vitro*, increased sensitivity to chemotherapy and extinguished multiple myeloma growth *in vivo*. EFNB2 reverse signaling represents an important new mechanistic target in multiple myeloma.

## Materials and Methods

### Cell lines and culture

Multiple myeloma cells (U266, NCI-H929, RPMI-8226) were purchased from ATCC and cultured in RPMI1640 medium containing 25 mmol/L HEPES, L-Glutamine (Thermo Fisher Scientific, 11875093) and 15% FBS. Cells were incubated in 37°C and 5% $CO_2$. Genetically modified cell lines were selected using antibiotic resistance and used for experimentation below passage 20 after engineering. Genetically engineered cells (shRNA, dCas9-VPR, and gRNA) were grown in media containing 4 μg/mL of puromycin (Sigma-Aldrich, P9620) and/or 8 μg/mL of blasticidin (Thermo Fisher Scientific, A1113903), depending on the resistance of the plasmids. BMEC-60 cells were provided courtesy of Dr. Ruben Carassco (Dana Farber Cancer Institute, Department of Pathology, Boston, MA; ref. 6). Human umbilical vein ECs (HUVEC) were provided courtesy of Dr. Shahin Rafii (Division of Regenerative Medicine, Weill Cornell Medicine, New York, NY; ref. 32). All other ECs were purchased from ATCC. Flasks or 24-well plates were precoated with 10% gelatin (Sigma Aldrich, G1393–100ML) for 30 minutes, then washed with PBS. BM ECs were cultured in EBM-2 Complete Culture Media (Lonza, CC-3156). Once they were 80% confluent, BM ECs were detached using a mixture of 0.05% Trypsin (Thermo Fisher Scientific, 25200056) and Versene (Thermo Fisher Scientific, 15040066) at a 1:8 ratio. This was inactivated with five times the volume of EBM-2 Complete Culture Media (Lonza). The cells were then centrifuged and passed at a 1:3 ratio. When in coculture conditions, cells were counted by flow cytometry using 123count eBeads Counting Beads (Thermo Fisher Scientific, 01–1234–42) according to the manufacturer's instructions. *Mycoplasma* testing was performed every 6 months using a PCR-based kit (ATCC, 30–1012K; latest test date August 23, 2023).

### Colony-forming cell assay

Multiple myeloma cells ($2 \times 10^3$) were seeded in 35-mm gridded culture dishes in MyeloCult M5300 media (StemCell Technologies, 05300) and colonies were scored at day 14.

### *In vitro* luciferase assay

Luciferin solution (50 μL) was added to cells in 24-well plates. RPMI-8226 cells that constitutively express firefly luciferase were utilized for these studies (courtesy of Dr. Alan Lichtenstein, Hematology/Oncology, VA West LA Hospital, Los Angeles, CA). Immediately after the addition of the substrate solution, luminescence was measured using a Luminoskan Ascent Luminometer with Ascent Software (Thermo Fisher Scientific).

### Viral transduction

A TC10 Cell counter was used to check the viability of the culture populations. All cell lines displayed viability > 95% before undergoing viral transduction. Forty thousand cells were placed in 96-well U-bottom tissue culture plates containing 200 mL of RPMI media supplemented with 1% FBS and 8 mg/mL of polybrene (Sigma Aldrich, TR-1003-G). Cells were plated with varying multiplicity of infections to determine optimal virus dose. At day 2, the virus was washed out and cells were replated with media containing 15% FBS. On day 4, the samples were transferred into selection media containing the appropriate antibiotic(s). The hEFNB2deltaC-EGFP construct was previously described (33), but it was in the pEGFP-N2 vector. The portion encoding hEFNB2deltaC-EGFP was subcloned into pLVX-IRES-Neo (using *Xho*I and *Not*I restriction sites) for use in these studies.

To silence *EPHB1* expression in human aortic ECs (HAEC), HAECs were cultured with complete endothelial cell growth medium (EBM-2 medium, Lonza) and cells were transfected with lentiviral particles that express human *EPHB1* shRNA or nontarget control shRNA and GFP marker (Horizon Discovery). Cells expressing shRNA and GFP were selected with 1 μg/mL puromycin (Sigma Aldrich, P7255–100MG).

### EC growth and angiogenesis assay

HAECs ($2.5 \times 10^4$ cells per well) transfected with *EPHB1* shRNA or nontarget shRNA were seeded in 6-well plates in triplicates in complete EBM-2 medium with 1 μg/mL puromycin. Viable cells were counted by Trypan blue exclusion on the indicated incubation time points and cell growth cure was plotted.

To measure EC angiogenesis, HAECs ($2.5 \times 10^4$ cells per well) transduced with *EPHB1* shRNA or nontarget shRNA were seeded in four replicates onto the top of the EC matrix in 96-well plate according to the instructions of the In Vitro Angiogenesis Assay Kit (Millipore Sigma, ECM625). EC matrix is a solid gel of basement proteins containing laminin, collagen type IV, heparan sulfate proteoglycans, entactin, and nidogen. It also contains various growth factors (TGFβ, FGF) and proteolytic enzymes (plasminogen, tPA, MMPs). HAECs were cultured at 37°C overnight. EC tube formation was inspected and photographed at 50x magnification using a Zeiss inverted light

microscope (Carl Zeiss Microscopy), and branch point counting was performed for quantification analysis.

### Expression analysis of human BM cells

Human BM cells from cadaveric donors not diagnosed with multiple myeloma were analyzed for *EFNB2* expression (Ossium Health) using Ficoll-Paque Plus (Thermo Fisher Scientific, 45–001–749), and washed with RPMI medium with 10% FBS. We sorted $CD11b^+$ myeloid cells, $CD269\ (BCMA)^+$ plasma cells, $CD3^+$ T cells, and $CD19^+$ B cells using anti-human CD3-BV421 (BioLegend, 317344), CD19-PE (BioLegend, 302208), CD269-AF647 (BioLegend, 357518), and CD11b-FITC (BioLegend, 982614) antibodies; cells were sorted using a BD Influx cell sorter (Becton Dickinson).

### qRT-PCR

As previously described (34), RNA isolation was performed using Qiagen Micro RNeasy Kits. RNA concentrations were measured with the Nanodrop 2000 Spectrophotometer (Thermo Fisher Scientific, ND-2000). Five-hundred nanograms of total RNA was reverse transcribed using the High Capacity cDNA Synthesis Kit (Thermo Fisher Scientific, 4368814). Real-time PCR reactions were conducted using TaqMan Universal PCR Master Mix (Thermo Fisher Scientific, 4304437) on an ABI Quant Studio 6-machine instrument with TaqMan predesigned gene expression assays (Thermo Fisher Scientific, 4331182; ref. 34). Primers and probes were produced by ABI and real-time PCR was performed on an ABI Quant Studio 6-machine instrument. All reactions were normalized using GAPDH.

### Flow cytometry and Annexin V analysis

BM cells were analyzed by flow cytometry to identify multiple myeloma cells and mouse leukocytes using the following antibodies: APC anti-human CD138 (BioLegend, 352308), APC anti-mouse CD138 (BioLegend, 142506), V450 Rat Anti-mouse CD45 (BD Biosciences, 56050), and PE anti-human CD34 (BD Biosciences, 550761). Discrimination of live and apoptotic cell fractions was performed by flow cytometry using the BD Annexin V-FITC Apoptosis Detection Kit (BD Biosciences, 556570), following the manufacturer's instructions. In addition, 7-amino-actinomycin (7AAD, BD Biosciences, 559925) staining was used to discriminate apoptosis (Annexin $V^+$ $7ADD^-$) from necrosis (Annexin $V^+$ $7ADD^+$). Data were analyzed on FACS Diva version 8 and FlowJo version 10 software.

### Phosflow

Multiple myeloma cells were incubated in serum-free media for 2 hours. Cells were stimulated with either human IgG1 mAb (R&D Systems, MAB9894-SP) or preclustered recombinant mouse EPHB4 Fc Chimera Protein (R&D Systems, 446-B4). Using a 1:1 ratio, human recombinant EPHB4 Fc (R&D Systems, 11307-B4) was preclustered with human IgG1 mAb for 30 minutes at room temperature. Cells were stimulated in a volume of 200 μL at 37°C for 15 minutes using a concentration of 10 μg/mL of EPHB4-Fc and IgG1. Following stimulation, 1 mL of prewarmed 1× Phosflow Lyse/Fix Buffer (BD Biosciences, 558049) was added and incubated for 10 minutes at 37°C. Cells were then washed and resuspended. Five-hundred microliters of Perm Buffer III (BD Biosciences, 558050) was added to each sample and placed on ice for 30 minutes. Samples were washed with 1 mL of Pharmingen Stain Buffer (BD Biosciences, 554656). Cells were separately stained with BD Phosflow Alexa Fluor 647 mouse anti-Stat3 (BD Biosciences, 557815) or Alexa Fluor 647 mouse anti-Stat5 (BD Biosciences, 612599). Cells were stained in the dark overnight at 4°C and analyzed using a FACSCanto (BD Biosciences). Isotype controls were used to delineate nonspecific binding.

### Bromodeoxyuridine analysis

Cells were incubated with bromodeoxyuridine (BrdU) for 6 hours and processed according to the manufacturer's protocol for the *in vitro* labeling of cells (BrdU BD Pharmingen BrdU Flow Kit, 559619). For inhibition of STAT5, cells were treated with 2-[(4-oxo-4H-1-benzopyran-3-yl)methylene]hydrazide 3-pyridinecarboxylic acid (MedChemExpress).

### Vk*MYC mouse model

Vk*MYC cells were obtained courtesy of Dr. Leif Bergsagel (Mayo Clinic, Scottsdale, AZ). All Vk*MYC studies were done in mice in a C57BL/6 background. Vk*MYC plasma cell clones were passed from mouse to mouse to preserve the line. Recipient C57BL/6 mice were injected via tail vein with $1–2 \times 10^5$ cells. Mice were sacrificed once a monoclonal protein band (M-protein) was detected on serum protein electrophoresis or upon signs of significant morbidity. All mice developed M-proteins by 4 to 6 weeks after tumor cell injection.

### Human multiple myeloma–NSG xenograft model

NSG mice (JAX strain no. 005557, The Jackson Laboratory) for human multiple myeloma xenograft studies were purchased from the Jackson Laboratory. Comparative survival studies of xenografted mice were done at least twice independently. A subset of mice were treated with anti-human EFNB2 single chain variable fragment (scFv)(B11) [TAB-390MZ-S(P), Creative BioLabs] or control antibody. Flow cytometric analyses were performed to detect human $CD138^+$ cells engrafted in the BM, peripheral blood, and vertebral bones; some samples were lost due to poor viability during processing and analysis. Mice were monitored daily for signs of morbidity. Mice were humanely euthanized when symptoms of morbidity such as weight loss ≥ 15%, immobility, or hunched posture were observed.

### Serum protein electrophoresis

Blood was collected from mice via submandibular venipuncture into Microtainer tubes (BD Biosciences, 365992), allowed to coagulate at room temperature, and spun for 10 minutes at $2{,}300 \times g$. Serum was diluted 1:2 in normal saline buffer and analyzed on a QuickGel Chamber apparatus using precasted QuickGels (Helena Laboratories, 1284), according to the manufacturer's instructions.

### Human patient samples

Primary multiple myeloma samples were obtained from BM aspirates of patients with multiple myeloma from the UCLA Ronald Reagan Medical Center under a UCLA Institutional Review Board (IRB)–approved protocol (principal investigator: Joshua Sasine, protocol no. 15–000062) after written informed consent was obtained from each patient. The study was performed in accordance with Declaration of Helsinki guidelines. Deidentified, healthy control BM samples were obtained from AllCells. BM microenvironment cells and $CD269^+$ (TNFRSF17/BCMA) multiple myeloma cells were isolated from primary human BM aspirates (34) as follows. Aspirates were diluted 1:1 in sterile PBS, layered over Ficoll-Paque density gradient medium (Thermo Fisher Scientific, 45–001–749) and centrifuged at 1,400 rpm for 30 minutes. Mononuclear cells were collected and column-enriched for $CD269^+$ cells using the Miltenyi Biotec human $CD269^+$ isolation kit (Miltenyi Biotec, 130–131–092). The negative cell fraction was plated in BMEC media to generate BM ECs from patients with multiple myeloma.

### ELISA

One-hundred microliters of mouse peripheral blood was collected in 1.5 mL Eppendorf tubes. After centrifugation, supernatants were collected and analyzed for human lambda light-chain protein levels using an ELISA kit (Thermo Fisher Scientific, E88–116), as per the manufacturer's instructions.

### RNA sequencing

RNA was isolated using Qiagen RNeasy Micro kit (Qiagen, 74104). Libraries for RNA-seq were prepared with Nugen Universal plus mRNA-Seq Kit to generate strand-specific RNA-seq libraries. The workflow consisted of poly(A) RNA selection, RNA fragmentation and double-stranded cDNA generation using a mixture of random and oligo(dT) priming, followed by end repair to generate blunt ends, adaptor ligation, strand selection, and PCR amplification to produce the final library. Different index adaptors were used for multiplexing samples in one sequencing lane. Sequencing was performed on NovaSeq 6000 for PE 2×150 bp run. Data quality check was done on Illumina SAV. Demultiplexing was performed with Illumina Bcl2fastq2 v 2.19.1.403 program. The Partek flow (Partek Inc.) was used for bioinformatics methods. Reads were mapped to the latest UCSC transcript set using STAR – 2.7.2a and GRCm38.97 (35). After obtaining gene counts, they were normalized by counts per million. The principal component analysis was applied to the transcript counts. The differential gene expressions were examined. Ingenuity Pathway Analysis (IPA) was used for data analysis (36). For all results of differential gene expression analysis, the *P* values and fold change (FC) filters were applied. The filter values were $P < 0.05$ and $|FC| > 2$ for all differential gene expression results.

### Microarray analysis

RNA was isolated using the QIAGEN RNeasy micro kit (QIAGEN). RNA was then sent to the UCLA Clinical Microarray Core (CMC) for processing. Total RNA was assessed for quality with Agilent 2100 Bioanalyzer G2939A (Agilent Technologies) and Nanodrop 8000 spectrophotometer (Thermo Scientific/Nanodrop). The samples were amplified using the NuGEN Ovation RNA Amplification System V2 (catalog no. 3100-A01; NuGEN Technologies Inc.) and were then hybridized to Affymetrix Human Genome U133 Plus 2.0 Array. Affymetrix GeneChip CEL files for the samples assayed were imported into the Affymetrix Expression Console software to perform gene level normalization and signal summarizations. Affymetrix Transcriptome Analysis Console (TAC) software was used to analyze the differential gene expression between the cell types. Robust multiarray average (RMA) values generated in the Affymetrix Expression Console software from this gene list were imported into Partek microarray data analysis software (Partek Inc.) and unsupervised hierarchical cluster analysis was performed on the various gene lists. For all results of differential gene expression analysis, statistical filters were applied: $P < 0.05$, FDR < 0.05, and $|FC| > 2$. Within the differentially expressed gene set, QIAGEN's IPA (QIAGEN, www.qiagen.com/ingenuity) was applied to identify enriched canonical pathways, diseases, and biological functions.

### Immunofluorescence imaging

Seven-week-old NSG mice were injected with $1 \times 10^7$ RPMI 8226 multiple myeloma cells at 24 hours following 180 cGy TBI. At week 3 and 5 posttransplant, mice were injected via tail vein with 20 μg AF647 VE-Cadherin antibody (BioLegend, 138006). One hour after antibody injection, mice were euthanized and femurs were collected. Femurs were fixed in 10 mL of 4% paraformaldehyde for 4 hours at 4°C. Femurs were then washed three times with PBS under agitation and then incubated in 10 mL of 0.5 mol/L EDTA solution (pH 7.4) for 24 hours under constant agitation at 4°C. After incubation, the bones were washed three times with PBS and then incubated in a cryoprotectant solution (10% sucrose, 1% PVP in PBS) for 24 hours at 4°C. Femurs were then embedded in OCT medium, frozen on dry ice, and then stored at −80°C. Sections (10 μm) were taken using a Leica CM3050 S. All slides were rehydrated with PBS, permeabilized with 0.30% Triton X-100 in PBS, and treated with a blocking solution (5% BSA, 5% goat serum in PBST). Slides were stained with primary antibodies to BCMA (1:250; R&D Biosystems, MAB107621, and BioLegend, 357518), EPHB4 (1:250, R&D Biosystems, MAB446), EFNB2 (1:100, Invitrogen, MA5–35098), and secondary antibodies against rat (1:1,000, Invitrogen, A11006) and rabbit (1:1,000, Invitrogen, A21428) and DAPI (Thermo Fisher Scientific, D1306). Slides were mounted using Dako Fluorescence Mounting Medium (Agilent, S302380–2). Imaging of femur sections was done on a Zeiss confocal microscope using a 63× objective.

Cytospins were performed on RPMI 8226 multiple myeloma cells and processed for confocal imaging. Slides dried overnight at room temperature and then fixed with 100% methanol for 10 minutes, followed by drying at room temperature for 2 hours. Cytospin slides were then processed identically to the femur slides, starting at rehydration with PBS.

### Clinical data analysis

Data were taken from two sources: The Multiple Myeloma Research Foundation (MMRF) CoMMpass trial and the Total Therapy Studies (37). Data from the Total Therapy trials were gathered from Oncomine. The MMRF CoMMpass trial included patients with newly diagnosed multiple myeloma with sufficient tumor material for the comprehensive analysis of each tumor genome and transcriptome. Patients were followed for their clinical outcomes longitudinally for a minimum of 8 years. The clinical study (NCT01454297) opened in July 2011 and includes dozens of sites in the United States and Canada that have enrolled hundreds of patients. The comprehensive analysis of each tumor and matched normal genome involved numerous analyses, among them was RNA sequencing (RNA-seq) to define transcript expression levels and fusion transcripts. An open-access, public clinical and molecular database, the CoMMpass Researcher Gateway (RG; https://research.themmrf.org), is available. Detailed methods used in these trials have been previously published (37–39).

### Statistical analysis

We utilized GraphPad Prism 6.0 for all statistical analyses and data are shown as means ± SD, unless otherwise indicated. The details of each experiment, including n values and type of statistical test used and *P* values, are shown in the figure legends. As previously described (34), data were verified for normal distribution and the statistical test utilized was based on the numbers of groups and variables. For one-way and two-way ANOVA analyses, *P* values were based on multiple test corrections. Sample sizes for *in vitro* studies were chosen based on observed effect sizes and SEs from prior studies. As we have previously described for animal studies (34), a power test was used to determine the sample size needed to observe a two-fold difference in means between groups with 0.8 power using a two-sided Student *t* test. Age-matched and sex-matched animals were utilized throughout. Investigators were not blinded and no animals were excluded from the analysis.

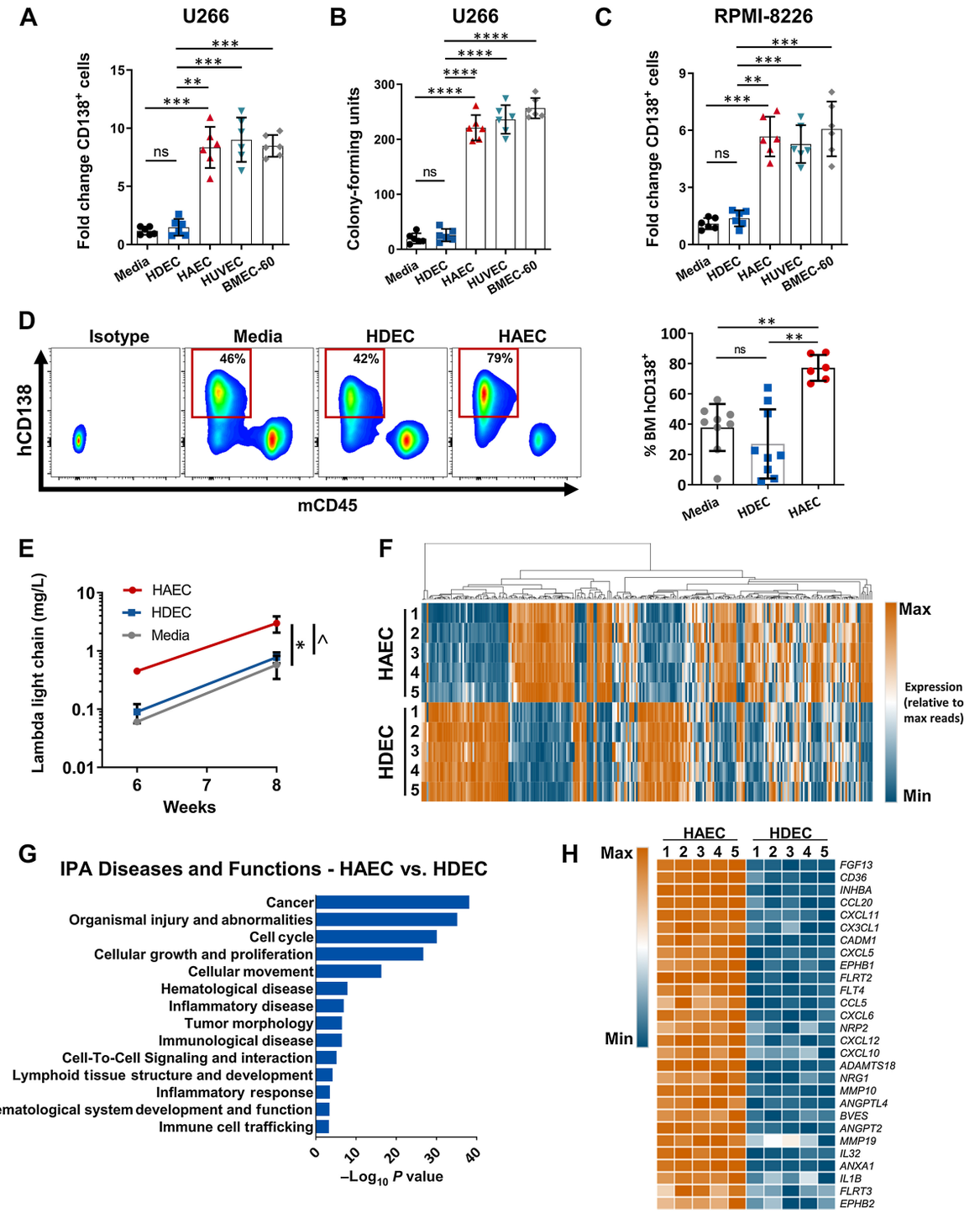


**Figure 1.**

Differential molecular analysis of human ECs that promote multiple myeloma (MM) growth. **A,** U266 multiple myeloma cells were cocultured with the human ECs shown for 7 days, then stained for CD138 and counted using flow cytometry. Fold change was normalized to media alone group. $n = 6$/group. **B,** Following the same conditions as in **A**, cells were placed into methylcellulose after 7 days and colony-forming cells were quantified. **C,** RPMI-8226 multiple myeloma cells were cocultured with ECs and counted as in **A**. $n = 6$/group. **D** and **E,** U266 multiple myeloma cells were cultured alone or with ECs for 7 days and then transplanted into NSG mice. A total of $1 \times 10^4$ multiple myeloma cells were cultured in 24-well plates with ECs and the culture progeny were transplanted. Disease burden was quantified on the basis of human $CD138^+$ (and mouse $CD45^-$) cells in the BM at 8 weeks and by quantification of PB human lambda light-chain levels over time. $n = 6$/group, AVOVA was used for light-chain analysis. **F,** Heat map of differentially expressed genes in HAECs versus HDECs. Heat map is relative to the maximum and minimum reads for each gene. **G,** IPA diseases and functions of HAEC versus HDEC. **H,** Heat map of selected EC candidate genes with increased expression in HAECs. One-way ANOVA and *post hoc t* test for all analyses. Error bars, SD. ns, not significant; *, $P < 0.05$; **, $P < 0.01$; ***, $P < 0.001$; ****, $P < 0.0001$.

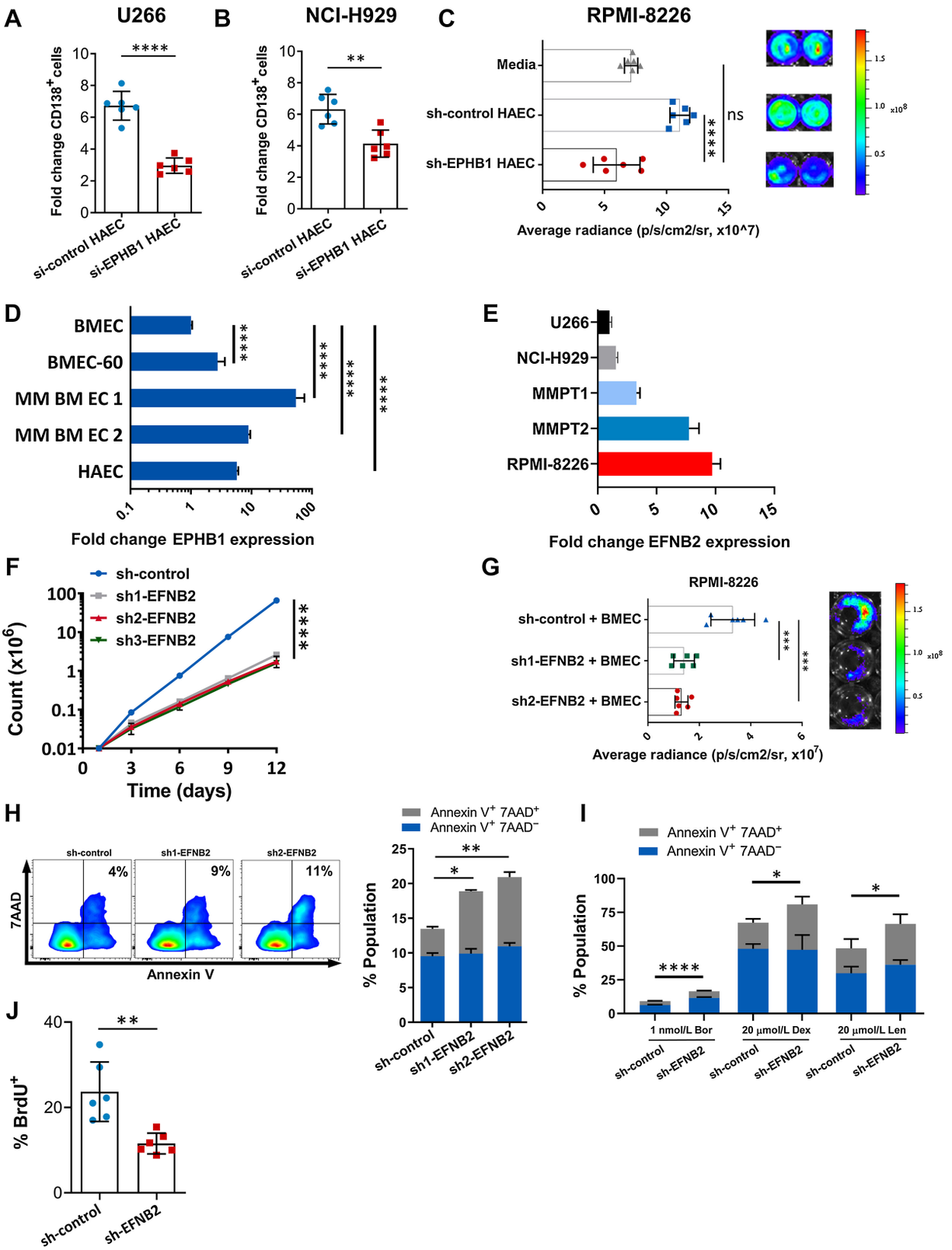
A
U266
Fold change CD138+ cells
si-control HAEC
si-EPHB1 HAEC
B
NCI-H929
C
RPMI-8226
Media
sh-control HAEC
sh-EPHB1 HAEC
ns
Average radiance (p/s/cm2/sr, x10^7)
D
BMEC
BMEC-60
MM BM EC 1
MM BM EC 2
HAEC
Fold change EPHB1 expression
E
U266
NCI-H929
MMPT1
MMPT2
RPMI-8226
Fold change EFNB2 expression
F
sh-control
sh1-EFNB2
sh2-EFNB2
sh3-EFNB2
Count (x10^6)
Time (days)
G
RPMI-8226
sh-control + BMEC
sh1-EFNB2 + BMEC
sh2-EFNB2 + BMEC
Average radiance (p/s/cm2/sr, x10^7)
H
sh-control
sh1-EFNB2
sh2-EFNB2
4%
9%
11%
7AAD
Annexin V
Annexin V+ 7AAD+
Annexin V+ 7AAD−
% Population
I
1 nmol/L Bor
20 µmol/L Dex
20 µmol/L Len
J
% BrdU+

### Study approval

All animal procedures were performed in accordance with Animal Use Protocol IACUC 009617 approved by the Cedars Sinai Animal Use Committee (principal investigator: J. Chute) and UCLA Protocol 2014–021–13M (principal investigator: J. Chute). All human sample acquisition and analyses were performed in accordance with UCLA IRB 15–000062-CR-00004 (principal investigator: J. Sasine), approved by the UCLA IRB.

### Data availability

Raw microarray data have been deposited at NCBI in the Gene Expression Omnibus (GEO) repository at GSE201846. Raw RNA-seq data for this study were generated at the UCLA Technology Center for Genomics and Bioinformatics. Derived data supporting the findings in the study are available in FigShare at hyperlink code https://figshare.com/projects/RNA-seq_of_Multiple_Myeloma_Cells_with_EFNB2_shRNA/191469. The data underlying all findings of these studies are available from the corresponding authors upon request and provided as separate source data files.

The clinical data analyzed in this study were obtained from The Multiple Myeloma Research Foundation (MMRF) CoMMpass trial at https://research.themmrf.org and the Total Therapy Studies (37) at Oncomine.

## Results

### Human ECs promote multiple myeloma cell growth *in vitro*

As a model to understand how ECs regulate multiple myeloma growth, we cocultured the human multiple myeloma cell line, U266 (ATCC), with different sources of human ECs. Coculture of U266 cells with HUVECs (32), HAECs, or the BM EC cell line, BMEC-60 (6), for 7 days caused a significant increase in $CD138^+$ multiple myeloma cells in culture and multiple myeloma colony-forming cells (40) compared with media alone, whereas coculture with human dermal ECs (HDEC) had no effect (**Fig. 1A** and **B**). We observed a similar level of expansion using RPMI-8226 multiple myeloma cells (**Fig. 1C**). To evaluate whether coculture with ECs could expand human multiple myeloma cells capable of reconstituting disease *in vivo*, we transplanted the progeny of $1\times10^4$ U266 cells at day 7 of coculture with HAECs or HDECs into NOD/SCID-IL2 receptor-gamma null (NSG) mice and compared with the progeny of the same dose of U266 cells cultured with media alone. At 8 weeks posttransplantation, mice transplanted with multiple myeloma cells cultured with HAECs displayed significantly increased engraftment with human $CD138^+$ multiple myeloma cells in the BM and approximately 10-fold increased human lambda light chain levels in the PB compared with mice transplanted with multiple myeloma cells cultured with HDECs or media alone (**Fig. 1D** and **E**).

Because HAECs differentially supported the expansion of multiple myeloma cells *in vitro*, we performed microarray analysis to identify genes with higher or lower expression in HAECs compared with HDECs. Microarray analyses revealed numerous differentially expressed genes in HAECs compared with HDECs (**Fig. 1F**; Supplementary Fig. S1A). IPA for diseases and functions demonstrated that genes involved in regulation of cancer, organismal injury, cell cycle, and cellular movement were most significantly enriched in the multiple myeloma–supportive HAECs (**Fig. 1G**). As an additional strategy to identify genes expressed by HAECs that were involved in promoting multiple myeloma growth, we filtered for secreted and cell surface proteins, and proteins for which a receptor is expressed by multiple myeloma cells. Several genes in this category were found to be upregulated in HAECs compared with HDECs, including genes that encode adhesion proteins, chemokines, cytokines, and growth factors (**Fig. 1H**).

### Expression of EPHB1 and EPHB4 in ECs regulates multiple myeloma cell growth

We utilized siRNA knockdown of specific genes that are overexpressed by HAECs coupled with coculture of $CD138^+$ multiple myeloma cells to identify HAEC genes important for supporting multiple myeloma growth. To avoid cell line–specific effects, we evaluated both U266 multiple myeloma cells and NCI-H929 multiple myeloma cells. Silencing the expression of several candidate genes in HAECs had no effect on multiple myeloma growth in coculture (Supplementary Fig. S1B) but silencing the expression of EPH receptor B1 (*EPHB1*) in HAECs suppressed multiple myeloma cell expansion in coculture (**Fig. 2A** and **B**). We validated the change in expression seen on the microarray using RT-PCR (Supplementary Fig. S1C and S1D) and siRNA knockdown (Supplementary Fig. S1E). Silencing *EPHB1* expression in HAECs using a lentiviral shRNA (*sh-EPHB1*, Supplementary Fig. S1F) also abrogated the expansion of RPMI-8226 multiple myeloma cells in a bioluminescence assay (41), compared with HAEC cocultures treated with *sh-Control* (**Fig. 2C**). More generally, we observed that silencing *EPHB1* suppressed HAEC growth in culture and inhibited the angiogenesis capacity of HAECs compared with *sh-Control*–treated HAECs (Supplementary Fig. S1G–S1I). Further analysis of primary human samples confirmed that *EPHB1* expression is relatively low in BM ECs from healthy donors but is significantly increased in BM ECs from patients with multiple myeloma (**Fig. 2D**).

We next tested whether *Ephb1* expression is also increased in BM ECs in transgenic *Vk*MYC* mice, which develop indolent myeloma as

**Figure 2.**

Loss of EPHB1–Ephrin B2 signaling impairs multiple myeloma pathogenesis. **A** and **B,** Mean fold change of $CD138^+$ cells in cocultures of U266 (**A**) and NCI-H929 (**B**) multiple myeloma (MM) cells with HAECs for 5 days. Multiple myeloma cells were treated with *si-EPHB1* or *si-Control*. Fold change is relative to input ($n$ = 6/group). **C,** Average radiance of RPMI-8226 multiple myeloma cells cocultured for 1 week with HAECs transduced with *sh-EPHB1* or *sh-Control*. Multiple myeloma cells were tagged with luciferase and luminescence was the readout for multiple myeloma cell expansion. $n$ = 6/group. **D,** Comparison of *EPHB1* expression by qRT-PCR across multiple human tissues: BMECs from a healthy donor (BMEC), the BMEC-60 cell line (BMEC-60), primary multiple myeloma patient ECs (multiple myeloma BM EC1 and 2) and HAECs. EPHB1 expression is shown relative to normal BM ECs and normalized using GAPDH. $n$ = 5/group. **E,** Expression of *EFNB2* in U266 multiple myeloma cells, NCI-H929 multiple myeloma cells, primary multiple myeloma patient cells (MMPT1 and 2), and RPMI-8226 multiple myeloma cells. Data represent fold change in expression by qRT-PCR following reverse transcription, normalized using GAPDH. Median value for U266 was used as a basis for relative expression. **F,** Cell counts of RPMI-8226 multiple myeloma cells over time, following treatment with shRNAs targeting EFNB2 (*sh-EFNB2*) or *sh-Control*. Cells were grown in absence of ECs. Results are mean ± SD using three independent shRNA sequences. $n$ = 5/group, analyzed with ANOVA. **G,** Average radiance of RPMI-8226 multiple myeloma cells at day 5 of coculture with BMECs following treatment with *sh-EFNB2* or *sh-Control*. $n$ = 6/group. **H,** Left, representative flow cytometric analysis of Annexin $V^+7AAD^+$ (necrotic) and Annexin $V^+7AAD^-$ (apoptotic) cells at 4 weeks of culture of RPMI-8226 multiple myeloma cells treated with *sh-EFNB2* or *sh-Control*. Right, mean levels of total Annexin $V^+$ cells within each treatment group. **I,** Mean percentages of Annexin $V^+$ cells within RPMI-8226 multiple myeloma cells treated with *sh-EFNB2* or *sh-Control* and exposed to bortezomib (Bor), dexamethasone (Dex), or lenalidomide (Len) for 24 hours. $n$ = 6/group. **J,** Mean $\%BrdU^+$ RPMI-8226 multiple myeloma cells after 4 hours of BrdU incubation under the conditions shown. *, $P < 0.05$; **, $P < 0.01$; ***, $P < 0.001$; ****, $P < 0.0001$.

a consequence of activation-induced deaminase-dependent MYC activation in germinal B cells (42, 43). We found that *Ephb1* expression is increased significantly in BM ECs from *Vk*MYC* mice that have active multiple myeloma compared with BM ECs from unaffected control mice (Supplementary Fig. S2A). Of note, BM ECs in *Vk*MYC* mice also displayed increased expression of *Ephb4* compared with BM ECs from control mice (Supplementary Fig. S2A). *EPHB4* was also the most highly expressed EPHB receptor in the human BM EC line, BMEC-60 (Supplementary Fig. S2B). shRNA-mediated silencing of *EPHB4* in BMEC-60 cells reduced the capacity of BMEC-60 cells to support multiple myeloma growth in coculture (Supplementary Fig. S2C and S2D).

### Silencing EFNB2 suppresses multiple myeloma growth

Both EPHB1 and EPHB4 are expressed by ECs and their signaling capacity is activated by binding to transmembrane ephrin B ligands expressed in adjacent cells (44). In the human genome, there are five EPHB receptors that bind to three transmembrane ephrin B ligands (44). Interactions are promiscuous within each A or B class of receptors and ligands. EPHB1, for example, regulates neuronal growth by binding EFNB2, but can also interact with other ephrin B ligands (45).

We detected expression of *EFNB2*, in three multiple myeloma cell lines and two primary multiple myeloma patient cell populations, whereas *EFNB1* was not detectable, and *EFNB3* was expressed at a low level in U266 cells (**Fig. 2E**; Supplementary Fig. S3A). Of note, analysis of cadaveric human BM cells revealed that *EFNB2* is highly expressed by human B and T cells, with lower expression in normal plasma cells, $CD34^+$ hematopoietic stem/progenitor cells and myeloid cells (Supplementary Fig. S3B). Because RPMI-8226 multiple myeloma cells displayed the highest levels of *EFNB2* expression, we treated RPMI-8226 cells with shRNAs targeting *EFNB2* (Supplementary Fig. S3C); this caused a nearly 70-fold reduction in growth of RPMI-8226 cells at day 12 of culture in all three conditions (**Fig. 2F**). Multiple myeloma cells also express *EPHB* receptors (Supplementary Fig. S3D and S3E), which could interact with EFNB2 and stimulate its reverse signaling capacity. Importantly, when we cultured human RPMI-8226 multiple myeloma cells harboring shRNA targeting *EFNB2* (*sh-EFNB2*) with BMEC-60 cells, this abrogated BMEC-60–mediated expansion of multiple myeloma cells in 5-day culture, showing that BM EC–mediated expansion of multiple myeloma cells in culture was dependent on EFNB2 signaling (**Fig. 2G**). Silencing *EFNB2* was also associated with increased multiple myeloma cell death compared with sh-control–treated multiple myeloma cells (**Fig. 2H**). Silencing *EFNB2* in multiple myeloma cells also augmented multiple myeloma cell death in 24-hour culture with antimyeloma therapies, including the proteasome inhibitor, bortezomib, dexamethasone, or the immunomodulatory drug, lenalidomide (**Fig. 2I**). Silencing *EFNB2* also decreased multiple myeloma proliferation measured by 4-hour BrdU incorporation (**Fig. 2J**).

### Inhibition of EFNB2 suppresses multiple myeloma growth *in vivo*

Because silencing *EPHB1* and *EPHB4* expression in ECs suppressed human multiple myeloma growth in coculture and inhibition of EFNB2 in human multiple myeloma cells inhibited multiple myeloma cell growth *in vitro*, we sought to determine whether EFNB2-expressing multiple myeloma cells would colocalize with EPHB-expressing BM ECs *in vivo*. We chose EPHB4 because it is the preferred binding partner for EFNB2 and is highly and specifically expressed on sinusoidal BM ECs (25). Immunofluorescence analysis of RPMI-8226 multiple myeloma cell cytospins demonstrated coexpression of B-cell maturation antigen (BCMA) and EFNB2 (**Fig. 3A**). To evaluate for *in vivo* colocalization, we transplanted NSG mice with $1 \times 10^7$ RPMI-8226 multiple myeloma cells at 24 hours post 180 cGy TBI and then immunostained femurs at 5 weeks. As shown in **Fig 3B**, VE-cadherin (Cdh5) and EPHB4 expression colocalized in BM ECs lining sinusoidal blood vessels in NSG mice (25). At 5 weeks posttransplant, $BCMA^+EFNB2^+$ multiple myeloma cells were detected abundantly and adjacent to $Cdh5^+$ blood vessels (**Fig. 3C**).

To determine whether inhibition of EFNB2 could affect multiple myeloma cell function *in vivo*, we transplanted NSG mice with $5 \times 10^6$ *sh-EFNB2*–treated RPMI 8226 multiple myeloma cells or equal dose of *sh-Control* multiple myeloma cells and measured multiple myeloma cell engraftment at 5 weeks. NSG mice transplanted with *sh-EFNB2*–treated multiple myeloma cells displayed significantly lower engraftment of human $CD138^+$ multiple myeloma cells compared with mice transplanted with *sh-Control*–treated multiple myeloma cells (**Fig. 3D**). This was associated with a significant increase in the percent survival of NSG mice transplanted with *sh-EFNB2*–treated multiple myeloma cells compared with that of mice transplanted with *sh-Control*–treated multiple myeloma cells (**Fig. 3E**).

Because silencing *EFNB2* expression suppressed multiple myeloma growth *in vivo*, we sought to determine whether administration of a highly specific single-chain variable fragment targeting EFNB2 (46) could also inhibit multiple myeloma cell growth. Treatment of RPMI-8226 cells *in vitro* with scFv-EFNB2 increased multiple myeloma cell death at 24 hours compared with control cultures (**Fig. 3F**). To evaluate the *in vivo* effects of scFv-EFNB2 in a human multiple myeloma xenograft model, we irradiated NSG mice with 180 cGy and injected $3 \times 10^6$ RPMI-8226 multiple myeloma cells via tail vein, followed by intravenous administration of scFv-EFNB2 (5 mg/kg) or vehicle on days +4, +6, +8, +10, and +12. At day +30, mice treated with scFv-EFNB2 displayed 50% lower engraftment of human $CD138^+$ multiple myeloma cells in the BM compared with control mice (**Fig. 3G**).

### EFNB2 expression promotes multiple myeloma survival, proliferation, and chemotherapy resistance

To understand the mechanisms through which EFNB2 promotes multiple myeloma growth, we performed RNA-seq on multiple myeloma cells treated with *sh-RNA-EFNB2* versus multiple myeloma cells treated with *sh-Control* (**Fig. 4A**; Supplementary Fig. S4A). Silencing *EFNB2* in RPMI-8226 cells caused the downregulation of several pathways including those involved in cellular movement, cell death and survival, cellular assembly, cell cycle, and DNA repair (Supplementary Fig. S4B). On the basis of the transcriptomic profiles of multiple myeloma cells treated with *shRNA-EFNB2* compared with multiple myeloma cells treated with *sh-Control*, RNA-seq Upstream Regulator IPA predicted various regulators that could be responsible for the transcriptomic differences, including E2F4, IFNG, CCND1, STAT1, E2F1, STAT3, CDKN1a, and STAT5a (**Fig. 4B**). Further analysis revealed that numerous STAT5 target genes were downregulated in multiple myeloma cells treated with *sh-EFNB2* (**Fig. 4C**). Of note, STAT proteins can be directly activated by ephrin B proteins (47–50), are drivers of multiple myeloma (51, 52), and associate with protection of multiple myeloma via the BM microenvironment (53–55). We found that silencing *EFNB2* in multiple myeloma cells decreased levels of phospho-STAT5 compared with *sh-Control*–treated multiple myeloma cells (**Fig. 4D**). Conversely, we did not detect a change in phospho-STAT3 or phospho-S6K in

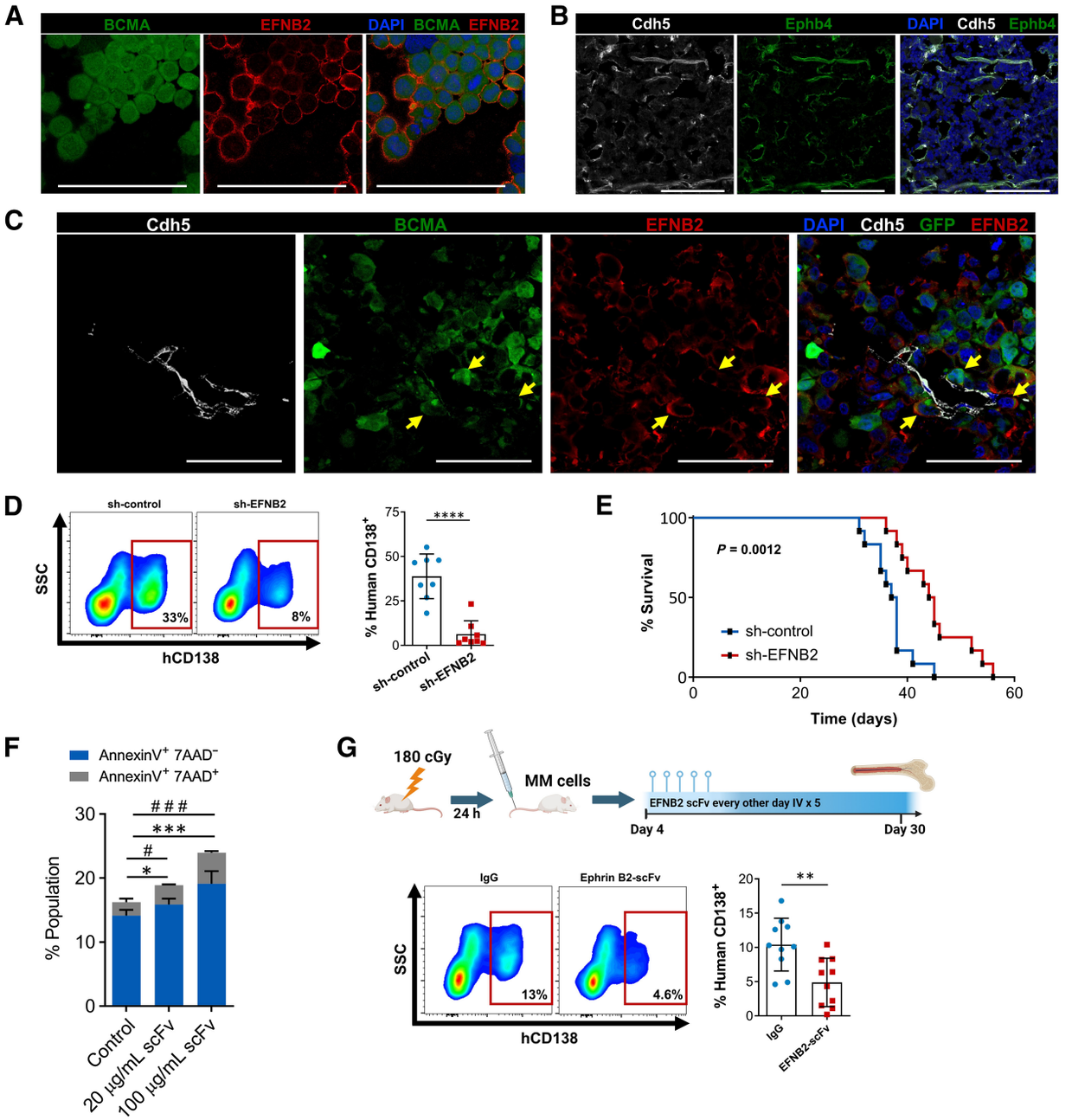


**Figure 3.**

Inhibition of ephrin B2 suppresses multiple myeloma growth *in vivo*. **A,** Representative immunofluorescence images of RPMI-8226 multiple myeloma (MM) cells stained for BCMA (green) and EFNB2; merged image with DAPI (blue) nuclear stain at right (red). Scale bar, 100 µm. **B,** Representative immunofluorescence images of VE-cadherin (Cdh5) expression (white) and Ephb4 colocalization (green) in BM blood vessels in NSG mice. Scale bar, 100 µm. **C,** Representative images of femur cross sections from NSG mice at 5 weeks posttransplant of RPMI-8226 multiple myeloma cells; sinusoidal blood vessel expressing VE-cadherin (Cdh5; white), multiple myeloma cells expressing BCMA (green), and EFNB2 (red) and merged image shown at right. Scale bar, 100 µm. Arrows, multiple myeloma cells adjacent to sinusoidal vessel. **D,** Left, representative flow cytometric analysis of human $CD138^+$ multiple myeloma cells in the BM of NSG mice at 5 weeks posttransplant of $5 \times 10^6$ RPMI-8226 cells treated with *sh-EFNB2* or *sh-Control*. SSC, side scatter. Right, mean percentages of $CD138^+$ multiple myeloma cells in the BM of transplanted mice. $n = 8$/group. **E,** Percent survival of NSG mice after transplantation of $5 \times 10^6$ RPMI-8226 cells transduced with *sh-EFNB2* or *sh-Control*. Log-rank test, $P = 0.0012$, $n = 12$/group. **F,** Mean percentages of Annexin $V^+$ RPMI-8226 cells at 24 hours posttreatment with EFNB2 scFv ($n = 6$/group). **G,** Top, schematic representation of experiment. Bottom left, representative flow cytometric analysis of human $CD138^+$ multiple myeloma cells in the BM of NSG mice at 4 weeks posttransplantation of $3 \times 10^6$ RPMI-8226 cells and intravenous administration of EFNB2 scFv or IgG on days +4, 6, 8, 10, and 12. Bottom right, mean percentages of $CD138^+$ multiple myeloma cells in the BM of transplanted mice. One-way ANOVA was utilized for analyses of three or more groups; Student two-sided *t* test was utilized otherwise. Error bars, SD. **, $P < 0.01$; ****, $P < 0.0001$; #, $P < 0.05$; ###, $P < 0.001$. (**G,** Created with BioRender.com.)

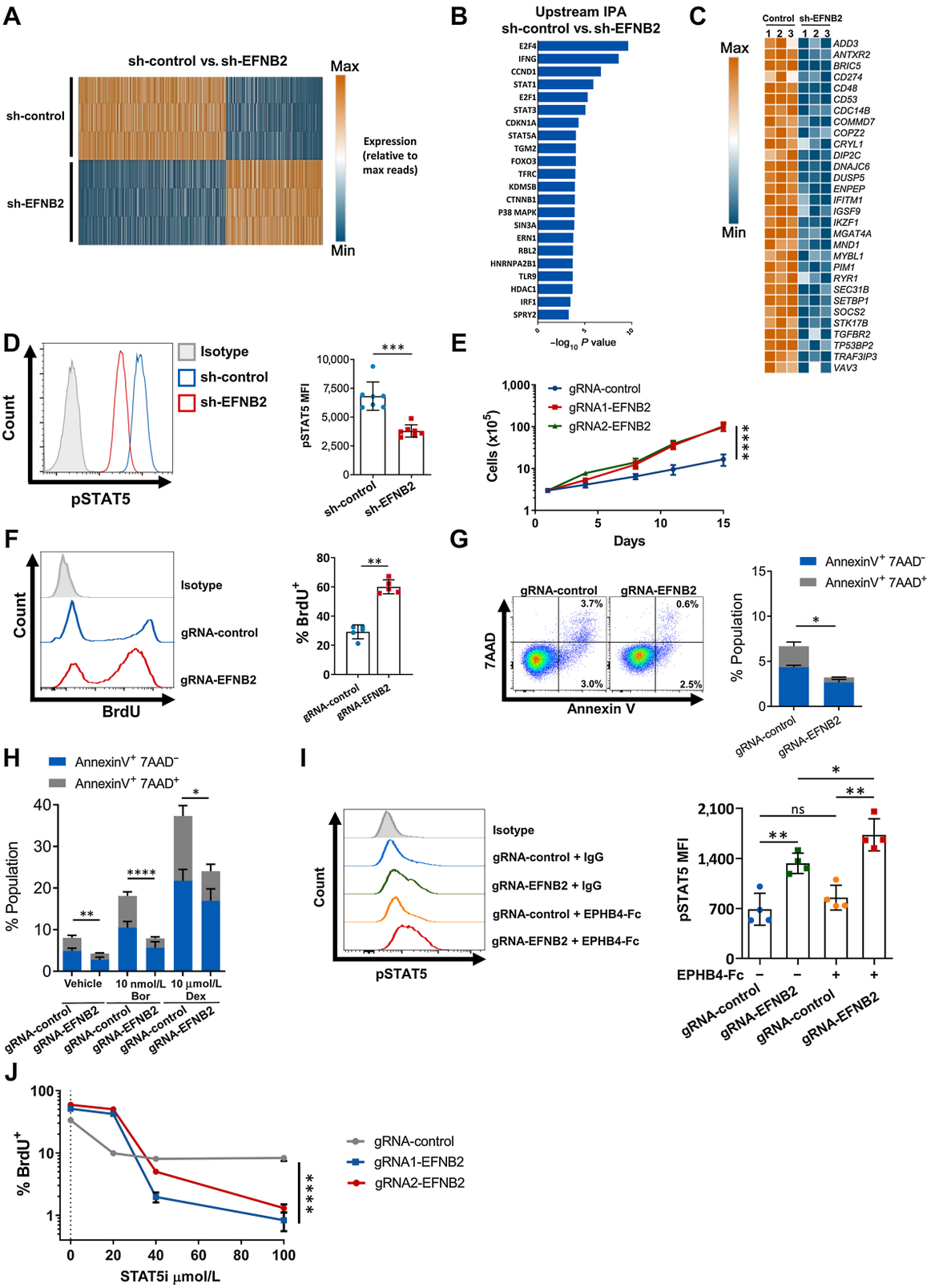
A
sh-control vs. sh-EFNB2
sh-control
sh-EFNB2
Max
Min
Expression (relative to max reads)
B
Upstream IPA
sh-control vs. sh-EFNB2
E2F4
IFNG
CCND1
STAT1
E2F1
STAT3
CDKN1A
STAT5A
TGM2
FOXO3
TFRC
KDM5B
CTNNB1
P38 MAPK
SIN3A
ERN1
RBL2
HNRNPA2B1
TLR9
HDAC1
IRF1
SPRY2
-log10 P value
C
Control
sh-EFNB2
1 2 3 1 2 3
Max
Min
ADD3
ANTXR2
BRIC5
CD274
CD48
CD53
CDC14B
COMMD7
COPZ2
CRYL1
DIP2C
DNAJC6
DUSP5
ENPEP
IFITM1
IGSF9
IKZF1
MGAT4A
MND1
MYBL1
PIM1
RYR1
SEC31B
SETBP1
SOCS2
STK17B
TGFBR2
TP53BP2
TRAF3IP3
VAV3
D
Isotype
sh-control
sh-EFNB2
Count
pSTAT5
pSTAT5 MFI
***
sh-control
sh-EFNB2
E
gRNA-control
gRNA1-EFNB2
gRNA2-EFNB2
Cells (x10^5)
Days
****
F
Isotype
gRNA-control
gRNA-EFNB2
Count
BrdU
% BrdU+
**
gRNA-control
gRNA-EFNB2
G
gRNA-control
gRNA-EFNB2
3.7%
0.6%
3.0%
2.5%
7AAD
Annexin V
AnnexinV+ 7AAD−
AnnexinV+ 7AAD+
% Population
*
gRNA-control
gRNA-EFNB2
H
AnnexinV+ 7AAD−
AnnexinV+ 7AAD+
% Population
**
****
*
Vehicle
10 nmol/L Bor
10 µmol/L Dex
gRNA-control
gRNA-EFNB2
gRNA-control
gRNA-EFNB2
gRNA-control
gRNA-EFNB2
I
Isotype
gRNA-control + IgG
gRNA-EFNB2 + IgG
gRNA-control + EPHB4-Fc
gRNA-EFNB2 + EPHB4-Fc
Count
pSTAT5
pSTAT5 MFI
*
**
ns
**
EPHB4-Fc
gRNA-control
gRNA-EFNB2
gRNA-control
gRNA-EFNB2
J
% BrdU+
gRNA-control
gRNA1-EFNB2
gRNA2-EFNB2
****
STAT5i µmol/L

response to silencing *EFNB2* in multiple myeloma cells (Supplementary Fig. S4C).

Because silencing *EFNB2* in multiple myeloma cells suppressed multiple myeloma growth *in vitro* and *in vivo*, we next examined whether enforcement of *EFNB2* expression in multiple myeloma cells could increase multiple myeloma pathogenesis. For *EFNB2* overexpression studies, we utilized the U266 multiple myeloma line that demonstrated the lowest level of *EFNB2* expression (**Fig. 2E**; Supplementary Fig. S5A) and overexpressed *EFNB2* via the CRISPR dCas9-VPR system (Supplementary Fig. S5B; ref. 56). Transduction of multiple myeloma cells with the dCas9-VPR and gRNA-EFNB2 caused a >30-fold increase in *EFNB2* expression (Supplementary Fig. S5C) that resulted in a 10-fold increase in multiple myeloma cells in 14-day culture compared with gRNA-control–treated multiple myeloma cells (**Fig. 4E**).

Multiple myeloma cell proliferation as measured by BrdU incorporation was also significantly increased in gRNA-EFN2 multiple myeloma cells compared with control multiple myeloma cells (**Fig. 4F**). In addition, gRNA-EFNB2 multiple myeloma cells displayed significantly decreased Annexin$^+$ apoptotic cells compared with gRNA-control multiple myeloma cells (**Fig. 4G**). Importantly, gRNA-EFNB2 multiple myeloma cells demonstrated markedly decreased sensitivity to chemotherapy agents, bortezomib and dexamethasone (**Fig. 4H**). At the molecular level, gRNA EFNB2 multiple myeloma cells demonstrated increased STAT5 phosphorylation compared with gRNA control multiple myeloma cells (**Fig. 4I**), and multiple myeloma cell proliferation in culture in response to EFNB2 overexpression was abrogated by treatment with a STAT5 inhibitor (**Fig. 4J**). These results suggest that EFNB2-mediated multiple myeloma growth is dependent on STAT5 activation. We did not detect a difference in STAT3 phosphorylation or phospho-SRC in multiple myeloma cells in response to enforced *EFNB2* expression (Supplementary Fig. S5D).

Our data demonstrate that EFNB2 expression strongly promotes multiple myeloma pathogenesis. To assess whether EFNB2 augmented multiple myeloma growth via forward signaling through its EPH receptor, we simultaneously silenced EPHB4 expression in gRNA-EFNB2 multiple myeloma cells. At 72 hours posttreatment with shRNA-EPHB4, we observed a modest increase in BrdU incorporation in gRNA-EFNB2 multiple myeloma cells compared with shRNA-control–treated cells (Supplementary Fig. S6A). However, gRNA-EFNB2 multiple myeloma cells treated with *shRNA-EPHB4* displayed no difference in cell growth compared with gRNA-EFNB2 multiple myeloma cells treated with *shRNA-control* (Supplementary Fig. S6B). We also observed no change in pSTAT5 levels in gRNA-EFNB2 multiple myeloma cells treated with *shRNA-EPHB4* compared with control cells (Supplementary Fig. S6C). These results suggest that EFNB2 does not augment multiple myeloma growth via forward signaling through EPHB4.

## EFNB2 reverse signaling controls multiple myeloma pathogenesis

We have shown that silencing of *EFNB2* expression suppresses multiple myeloma growth *in vitro* and *in vivo*, but this approach does not discriminate whether EFNB2 forward or reverse signaling is the essential mechanism of action. To determine whether EFNB2 forward or reverse signaling predominates in multiple myeloma, we used a mutant *EFNB2* construct (delta cytoplasmic EFNB2, dEFNB2; **Fig. 5A**), encoding EFNB2 residues 1–265, which includes the extracellular region, transmembrane helix and the first 15 residues of the intracellular region; dEFNB2 lacks the cytoplasmic portion responsible for reverse signaling, which is replaced by EGFP (33). We transduced U266 multiple myeloma cells with dEFNB2 or control vector and measured multiple myeloma pathogenicity. U266 multiple myeloma cells transduced with dEFNB2 displayed decreased cell growth in culture compared with control multiple myeloma cells (**Fig. 5B**). Commensurate with this, dEFNB2 expression repressed BrdU incorporation in multiple myeloma cells (**Fig. 5C**). Expression of dEFNB2 also substantially increased multiple myeloma cell death and suppressed STAT5 activation compared with control multiple myeloma cells (**Fig. 5D** and **E**).

To evaluate the therapeutic relevance of inhibiting EFNB2 reverse signaling in multiple myeloma cells, we measured multiple myeloma cell apoptosis during 24-hour culture with and without bortezomib or dexamethasone, coupled with dEFNB2 transduction. The combination of dEFNB2 expression and bortezomib treatment caused approximately three times increased multiple myeloma cell death compared with bortezomib alone (**Fig. 5F**; Supplementary Fig. S6D). Similarly, dEFNB2 expression coupled with dexamethasone treatment nearly doubled multiple myeloma cell death compared with dexamethasone alone (**Fig. 5F**). These results suggest that blockade of EFNB reverse signaling is mechanistically nonredundant with bortezomib and dexamethasone effects and appears to synergize with proteasome inhibitors for the treatment of human multiple myeloma. These data also suggest a dominant-negative effect caused by the competition of overexpressed dEFNB2 with endogenously expressed EFNB2 for binding to EPHB receptors, resulting in inhibition of endogenous EFNB2 reverse signaling.

To determine the effect of silencing EFNB2 reverse signaling on multiple myeloma growth *in vivo*, we compared the repopulation of U266 multiple myeloma cells following transplantation into NSG mice. NSG mice transplanted with $1 \times 10^5$ U266 multiple myeloma cells (transduced with GFP control) engrafted robustly, with mean > 60% CD138$^+$GFP$^+$ multiple myeloma cell engraftment detected at 8 weeks posttransplant (**Fig. 5G**). In contrast, mice transplanted with an equal dose of U266 multiple myeloma cells transduced with dEFNB2 displayed < 0.1% CD138$^+$GFP$^+$ multiple myeloma cell

**Figure 4.**

The effects of ephrin B2 on multiple myeloma are mediated by STAT5. **A,** Heat map of differentially expressed genes by RNA-seq of *sh-EFNB2* versus *sh-Control* cells. **B,** Upstream regulator analysis from IPA of RNA-seq data. **C,** Selected STAT5 target genes in the RNA-seq data. **D,** Left, representative analysis of phospho-STAT5 in RPMI-8226 cells treated with *sh-EFNB2* or *sh-Control* in presence of EPHB4-Fc. Right, mean fluorescence intensity (MFI) of pSTAT5 in the *sh-EFNB2*- and *sh-Control*–treated multiple myeloma cells. **E,** Numbers of U266 cells in culture over time when transduced with *gRNA1-EFNB2* and *gRNA2-EFNB2*. **F,** Left, representative histograms of BrdU incorporation over 6 hours in U266 cells transduced with the labeled construct. Right, %BrdU$^+$ cells in each group. **G,** Left, representative flow cytometric analysis of Annexin V$^+$7AAD$^+$ (necrotic) and Annexin V$^+$7AAD$^-$ (apoptotic) cells. Right, mean levels of total Annexin V$^+$ cells within each treatment group. **H,** Mean percentages of Annexin V$^+$ U266 cells engineered with the indicated construct and exposed to bortezomib (Bor) or dexamethasone (Dex) for 24 hours. $n = 6$/group. **I,** Representative histograms of p-STAT5 in U266 cells transduced with *gRNA-EFNB2* or *gRNA-control*, with and without stimulation by EPHB4-Fc. IgG (isotype) was used as a negative control for EPHB4-Fc. Right, mean MFI of pSTAT5 in each treatment population. **J,** Multiple myeloma cells transduced with *gRNA-EFNB2* or *gRNA-control* were cultured with increasing concentrations of the STAT5 inhibitor 2-[(4-oxo-4H-1-benzopyran-3-yl)methylene]hydrazide 3-pyridinecarboxylic acid (STAT5i) for 24 hours, then BrdU incorporation analysis was performed. $n = 6$/group. One-way ANOVA used for analyses in which there were three or more groups, Student two-sided *t* test for the other analyses. Error bars, SD. ns, not significant; *, $P < 0.05$; **, $P < 0.01$; ***, $P < 0.001$; ****, $P < 0.0001$.

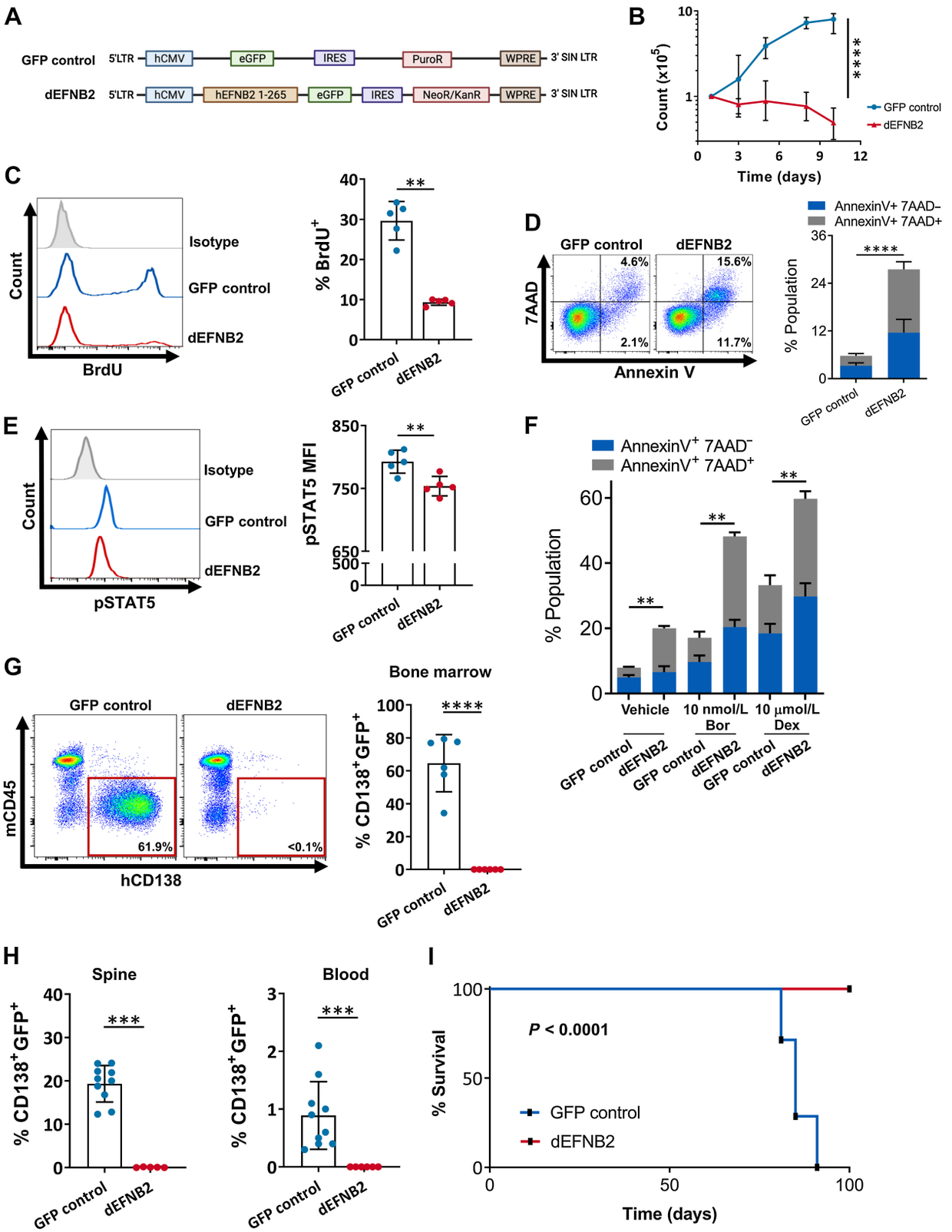
A
GFP control
5'LTR
hCMV
eGFP
IRES
PuroR
WPRE
3' SIN LTR
dEFNB2
5'LTR
hCMV
hEFNB2 1-265
eGFP
IRES
NeoR/KanR
WPRE
3' SIN LTR
B
Count (x10^5)
Time (days)
GFP control
dEFNB2
****
C
Count
BrdU
Isotype
GFP control
dEFNB2
% BrdU+
**
GFP control
dEFNB2
D
GFP control
dEFNB2
7AAD
Annexin V
4.6%
15.6%
2.1%
11.7%
AnnexinV+ 7AAD–
AnnexinV+ 7AAD+
% Population
****
GFP control
dEFNB2
E
Count
pSTAT5
Isotype
GFP control
dEFNB2
pSTAT5 MFI
**
GFP control
dEFNB2
F
AnnexinV+ 7AAD–
AnnexinV+ 7AAD+
% Population
**
**
**
Vehicle
10 nmol/L Bor
10 µmol/L Dex
GFP control
dEFNB2
GFP control
dEFNB2
GFP control
dEFNB2
G
GFP control
dEFNB2
mCD45
hCD138
61.9%
<0.1%
Bone marrow
% CD138+GFP+
****
GFP control
dEFNB2
H
Spine
% CD138+GFP+
***
GFP control
dEFNB2
Blood
% CD138+GFP+
***
GFP control
dEFNB2
I
% Survival
P < 0.0001
GFP control
dEFNB2
Time (days)

engraftment at 8 weeks, suggesting that EFNB2 reverse signaling is essential for multiple myeloma repopulation *in vivo* (**Fig. 5G**). Analysis of PB and thoracic spine of transplanted mice also demonstrated nearly undetectable $CD138^+GFP^+$ multiple myeloma cells in mice transplanted with dEFNB2-expressing multiple myeloma cells compared with mice transplanted with equal doses of control multiple myeloma cells (**Fig. 5H**). Commensurate with these results, PB lambda light-chain levels were significantly lower in mice transplanted with dEFNB2-expressing multiple myeloma cells compared with mice transplanted with control multiple myeloma cells (Supplementary Fig. S6E). Survival studies demonstrated 100% survival of NSG mice transplanted with dEFNB2-treated multiple myeloma cells, whereas no mice transplanted with GFP control multiple myeloma cells survived to 100 days (**Fig. 5I**).

### EFNB2 expression is associated with poor prognosis in multiple myeloma

Because our studies suggested that EFNB2 signaling regulates multiple myeloma cell growth and survival, we interrogated publicly available databases to determine whether *EFNB2* expression is associated with specific outcomes in patients with multiple myeloma. Reviewing the Total Therapy 2 and 3 studies (37) and the CoMMpass data (Multiple Myeloma Research Foundation, https://research.themmrf.org/, accessed on October 20, 2021; $n = 773$ patients), we discovered that *EFNB2* expression was increased in tumors from higher risk cytogenetic categories, including the t(4;14) translocation and gain of chromosome 1q populations (**Fig. 6A** and **B**). Conversely, the favorable risk ("standard risk") category, hyperdiploid multiple myeloma, displayed lower *EFNB2* expression (**Fig. 6C**). Stage III multiple myeloma also demonstrated higher *EFNB2* levels compared with stage I or II disease (**Fig. 6D**). Increased expression of *EFNB2* is also associated with decreased survival in patients with multiple myeloma (**Fig. 6E**). Among patients in the CoMMpass trial, those with the highest decile of *EFNB2* expression demonstrated decreased progression-free survival and decreased overall survival compared with all other patients (**Fig. 6F** and **G**). These results suggest that *EFNB2* expression is a poor prognostic marker in patients with multiple myeloma. Of note, analysis of the Total Therapy dataset did not demonstrate an association between EPHB1 or EPHB4 expression and prognosis in multiple myeloma.

## Discussion

These studies provide the first evidence that EFNB2 reverse signaling is essential for multiple myeloma growth and pathogenesis. Ephrins are a class of cell-membrane bound ligands for the EPH receptor tyrosine kinases with demonstrated functions in regulating mammalian development (57, 58), axon regeneration (59, 60), and angiogenesis (33). Ephrin–EPH receptor signaling is unique in that both forward signaling through the EPH receptor and reverse signaling through the ephrin can occur in cells (44, 57, 61). EPH–Ephrin signaling has also been shown to be promiscuous within EPH receptor–Ephrin A or B subclasses (62). Preliminary studies have suggested a potential role for ephrins in regulating the pathogenesis of glioblastoma, melanoma, breast cancer, and other cancers (44, 49, 63, 64), and in regulating the BM microenvironment response to multiple myeloma in immune-deficient mice (65). EPHA3 expression was shown to be upregulated in BM ECs from patients with multiple myeloma and in multiple myeloma cells, and silencing EPHA3 expression inhibited both the angiogenic capacity of myeloma patient–derived ECs and the adhesion and growth of multiple myeloma cells (66, 67). *In vitro* studies also showed that multiple myeloma cells express EPHA4 and that EPHA4 regulates multiple myeloma cell adhesion and proliferation via activation of Akt signaling (68). Our studies provide evidence that ephrin B2 reverse signaling directly promotes multiple myeloma pathogenesis and that targeted inhibition of ephrin B2 reverse signaling abolishes multiple myeloma growth *in vivo*.

In our gene expression analysis of human ECs that support multiple myeloma growth *in vitro* and *in vivo*, we identified *EPHB1* and *EPHB4* as overexpressed in multiple myeloma–supportive ECs. In complementary studies, we determined that the gene encoding one of the cognate ligands for EPHB1 and EPHB4, EFNB2, is upregulated in multiple myeloma cell lines and primary multiple myeloma cells from patients. These results suggest that vascular ECs may drive multiple myeloma pathogenesis via activation of EFNB2 reverse signaling through high expression of EPHB receptors. EFNB2 reverse signaling has been shown to promote colorectal cancer chemoresistance and progression through activation of the Src–ERK pathway (69). Similarly, activation of EFNB2 reverse signaling has been implicated in the progression of oral squamous cell carcinoma (70), glioblastoma (64, 71), and perivascular invasion and migration, in part by mediating anchorage-independent cytokinesis through RhoA (72). Here, silencing *EFNB2* expression in multiple myeloma cells inhibited multiple myeloma survival and proliferation, increased sensitivity to chemotherapy and abrogated multiple myeloma cell engraftment *in vivo*. However, silencing of *EFNB2* expression could suppress forward and reverse signaling in multiple myeloma cells, so this approach did not resolve which EFNB2 signaling pathway was the dominant mechanism of multiple myeloma pathogenesis.

Forward signaling via Ephrin–EPHB interactions has been shown to regulate EC function and vasculogenesis, which could contribute to multiple myeloma pathogenesis. Specifically, EPHB2 and EPHB4 are required for vascular morphogenesis and EC chemotaxis in response to SDF-1 gradients (73). EFNB2-mediated activation of EPHB2 or EPHB4 forward signaling has also been shown to augment EC chemotaxis in response to SDF-1 (73). Utilizing an implant angiogenesis mouse

**Figure 5.**

Loss of ephrin B2 reverse signaling abrogates multiple myeloma pathogenesis. **A,** Plasmid maps of overexpression constructs for dEFNB2 mutant lacking the cytoplasmic reverse signaling domain and GFP control. **B,** Numbers of U266 cells in culture over time when transduced with dEFNB2 or GFP control. **C,** Left, representative histograms of BrdU incorporation over 6 hours in U266 cells transduced with the labeled construct. Right, $\%BrdU^+$ cells in each group. **D,** Left, representative flow cytometric analysis of Annexin V and 7AAD staining of multiple myeloma cells transduced with dEFNB2 or GFP control; right, mean levels of total Annexin $V^+/7AAD^-$ cells and Annexin $V^+/7AAD^+$ cells within each treatment group. **E,** Left, representative histograms of phospho-STAT5 in U266 cells transduced with the labeled construct. Right, quantified phospho-STAT5 mean fluorescence intensity (MFI) in each group. **F,** Mean percentages of Annexin $V^+$ U266 cells engineered with the indicated construct and exposed to bortezomib (Bor) or dexamethasone (Dex) for 24 hours. $n = 6$/group. **G,** Left, representative flow cytometric analysis of human $CD138^+GFP^+$ multiple myeloma cells in the BM of NSG mice at 7 weeks posttransplant of $1 \times 10^5$ U266 cells transduced with dEFNB2 or GFP control. Right, mean percentages of human $CD138^+GFP^+$ multiple myeloma cells in the BM of transplanted mice. $n = 6$–7/group. **H,** Mean percentages of $CD138^+GFP^+$ multiple myeloma cells in the spine and PB in NSG at 7 weeks after transplantation of U266 cells transduced with dEFBN2 or GFP control ($n = 5$–10/group). **I,** Survival of NSG mice transplanted with $1 \times 10^5$ dEFNB2-treated multiple myeloma cells or GFP control multiple myeloma cells ($n = 10$ control; $n = 11$ dEFNB2 mice). One-way ANOVA was used for analyses in which there were three or more groups, Student two-sided $t$ test for the other analyses. Error bars, SD. **, $P < 0.01$; ***, $P < 0.001$; ****, $P < 0.0001$.

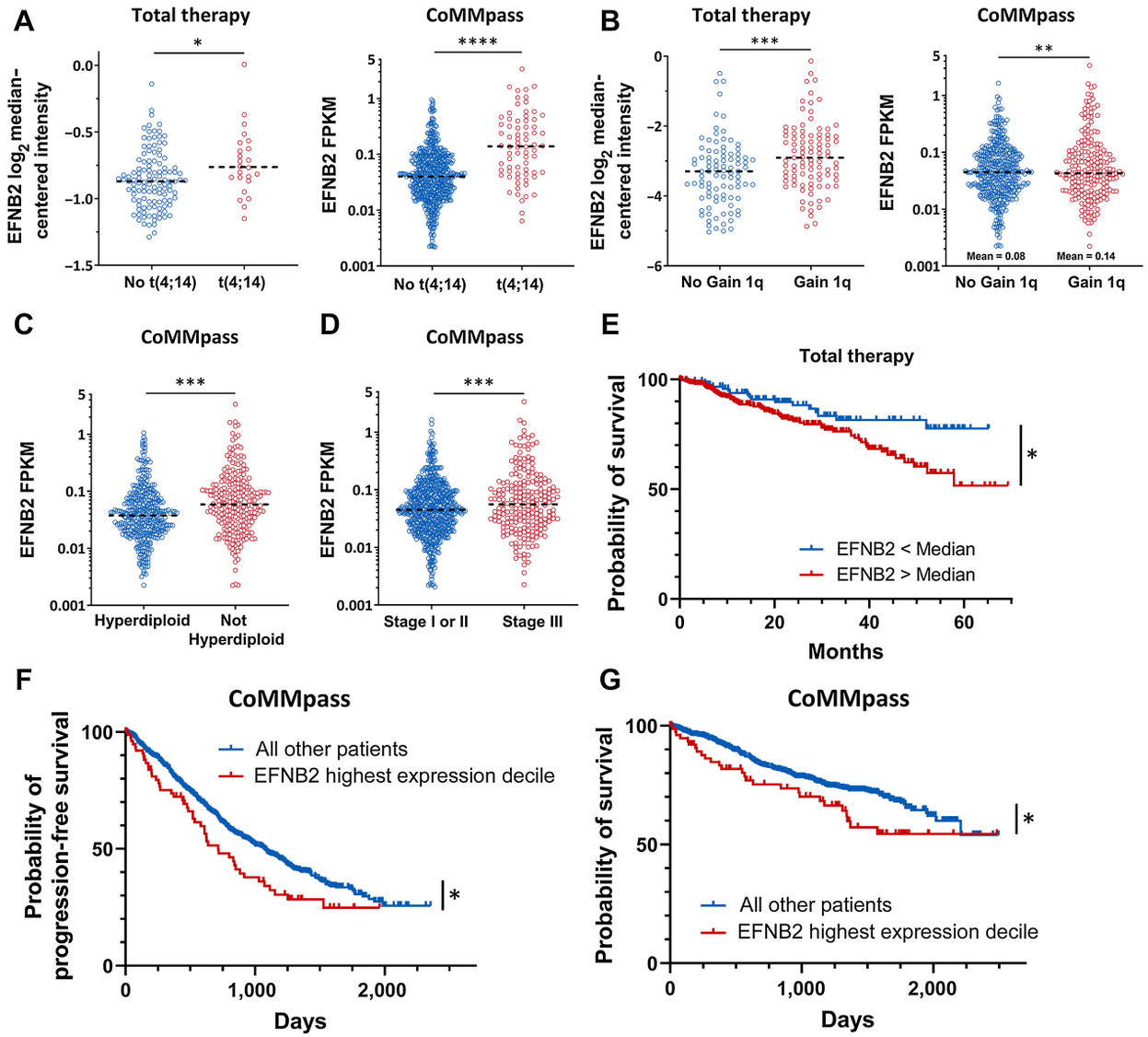


**Figure 6.**

Ephrin B2 expression associates with clinical outcomes in patients with multiple myeloma. **A–D,** *EFNB2* expression in patients with t(4;14) (**A**), amplification of chromosome 1q (**B**), hyperdiploid multiple myeloma (**C**), and high-stage disease (**D**) in two independent clinical studies. **E,** Patients with multiple myeloma expressing *EFNB2* above the median had decreased survival in the Total Therapy 2 and 3 trials. Log-rank analysis, $P = 0.024$. **F** and **G,** A patient cohort in the CoMMpass data defined by the highest decile of *EFNB2* expression has decreased progression-free survival (**F**) and overall survival (**G**). Log-rank analysis, $P = 0.013$ and 0.034, respectively. Student two-sided *t* test for all analyses unless otherwise stated. Error bars, SD. *, $P < 0.05$; **, $P < 0.01$; ***, $P < 0.001$; ****, $P < 0.0001$.

model, systemic administration of an EPHB4 kinase inhibitor was shown to inhibit VEGF-driven vessel angiogenesis *in vivo* (74). To resolve the precise contributions of EFNB2 reverse signaling and forward signaling in multiple myeloma, we utilized a mutant dEFNB2, which lacks reverse signaling capacity (33). We discovered that specific inhibition of EFNB2 reverse signaling in multiple myeloma cells increased multiple myeloma cell death, decreased proliferation, increased sensitivity to chemotherapy, and eliminated multiple myeloma growth *in vivo*. Conversely, shRNA-mediated silencing of *EFNB2* in multiple myeloma cells, which interrupts EFNB2-reverse signaling and EFNB-forward signaling through EPHB receptors, slowed multiple myeloma disease progression *in vivo*, but all mice ultimately succumbed to multiple myeloma. These results suggest that EFNB2-mediated forward signaling through EPHB receptors may negatively regulate multiple myeloma growth. Taken together, our data demonstrate conclusively that EFNB2 reverse signaling drives multiple myeloma pathogenesis.

In summary, we have provided anatomic and functional evidence that suggests the importance of EPHB4–Ephrin B2 reverse signaling in EC-mediated regulation of multiple myeloma pathogenesis. Furthermore, targeted inhibition of ephrin B2 reverse signaling in multiple myeloma cells abolishes multiple myeloma growth in preclinical models. Corresponding clinical data suggest that that ephrin B2 expression correlates with adverse prognosis in patients with multiple

myeloma. Given the substantial progress that has been made in the development of decoy proteins and single-chain variable fragments that target EPHB4 and ephrin B2, respectively (46, 75), the ephrin B2–reverse signaling pathway represents an important new mechanistic and therapeutic target in multiple myeloma.

## Authors' Disclosures

J.P. Sasine reports personal fees from Kite Pharma/Gilead, Genmab, and personal fees from Autolus outside the submitted work. E.B. Pasquale reports grants from NIH during the conduct of the study; in addition, E.B. Pasquale has a patent 7999069 issued, a patent 20100183510 issued, and a patent 7582438 issued. J.P. Chute reports grants from National Institute of Allergy and Infectious Diseases and grants from National Heart, Lung, and Blood Institute during the conduct of the study. No disclosures were reported by the other authors.

## Authors' Contributions

**J.P. Sasine:** Conceptualization, formal analysis, investigation, writing–original draft, writing–review and editing. **N.Y. Kozlova:** Formal analysis, investigation, methodology. **L. Valicente:** Formal analysis, investigation. **J. Dukov:** Formal analysis, investigation. **D.H. Tran:** Formal analysis, investigation. **H.A. Himburg:** Formal analysis, investigation, writing–original draft. **S. Kumar:** Formal analysis, visualization. **S. Khorsandi:** Formal analysis, investigation. **A. Chan:** Formal analysis, investigation. **S. Grohe:** Formal analysis, investigation. **M. Li:** Formal analysis, investigation. **J. Kan:** Formal analysis, investigation. **M.E. Sehl:** Resources, investigation. **G.J. Schiller:** Resources, writing–review and editing. **B. Reinhardt:** Formal analysis, investigation. **B.K. Singh:** Resources, investigation. **R. Ho:** Resources, investigation. **P. Yue:** Formal analysis, investigation. **E.B. Pasquale:** Resources, writing–review and editing. **J.P. Chute:** Conceptualization, resources, supervision, funding acquisition, methodology, writing–original draft, writing–review and editing.

## Acknowledgments

We thank Dr. Christina Termini and Dr. Yuwei He for their expertise regarding immunofluorescence microscopy, Dr. Ruben Carassco for providing the BMEC-60 cell line, Dr. Leif Bergsagel for providing the Vk*MYC cells, Mike Matsumoto for generating the dEFNB2 construct, and Edo Israely for assistance with cell sorting. This work was supported by funding from the NIH grant K08CA245483 (to J.P. Sasine), NIH grant UL1TR001881 (to J.P. Sasine), NIH grant NHLBI HL086998 (to J.P. Chute), NIH grant NIAID U01 AI156922 (to J.P. Chute), Tower Cancer Research Foundation Career Development Award (to J.P. Sasine), and the ASCO Young Investigator Award (to J.P. Sasine).

## Note

Supplementary data for this article are available at Cancer Research Online (http://cancerres.aacrjournals.org/).

Received June 30, 2023; revised November 14, 2023; accepted January 11, 2024; published first January 17, 2024.

## References

1. Surveillance Epidemiology and End Results (SEER) Program. Surveillance Epidemiology and End Results (SEER) Program (https://seer.cancer.gov/) SEER*Stat Database: Populations - Total U.S. (1969–2014) <csingle ages to 85+, Katrina/Rita Adjustment>- linked to county attributes - Total U.S., 1969–2014 Counties, National Cancer Institute, DCCPS, Surveillance Research Program, Surveillance Systems Branch, October 2015.
2. Teras LR, DeSantis CE, Cerhan JR, Morton LM, Jemal A, Flowers CR. 2016 US lymphoid malignancy statistics by World Health Organization subtypes. CA Cancer J Clin 2016;66:443–59.
3. Abe M, Hiura K, Wilde J, Shioyasono A, Moriyama K, Hashimoto T, et al. Osteoclasts enhance myeloma cell growth and survival via cell-cell contact: a vicious cycle between bone destruction and myeloma expansion. Blood 2004;104:2484–91.
4. Ribatti D, Nico B, Vacca A. Multiple myeloma as a model for the role of bone marrow niches in the control of angiogenesis. Int Rev Cell Mol Biol 2015;314:259–82.
5. Roccaro AM, Sacco A, Maiso P, Azab AK, Tai YT, Reagan M, et al. BM mesenchymal stromal cell-derived exosomes facilitate multiple myeloma progression. J Clin Invest 2013;123:1542–55.
6. Zhu D, Wang Z, Zhao JJ, Calimeri T, Meng J, Hideshima T, et al. The Cyclophilin A-CD147 complex promotes the proliferation and homing of multiple myeloma cells. Nat Med 2015;21:572–80.
7. Ferrucci A, Moschetta M, Frassanito MA, Berardi S, Catacchio I, Ria R, et al. A HGF/cMET autocrine loop is operative in multiple myeloma bone marrow endothelial cells and may represent a novel therapeutic target. Clin Cancer Res 2014;20:5796–807.
8. Chen Z, Orlowski RZ, Wang M, Kwak L, McCarty N. Osteoblastic niche supports the growth of quiescent multiple myeloma cells. Blood 2014;123:2204–8.
9. Frassanito MA, Rao L, Moschetta M, Ria R, Di Marzo L, De Luisi A, et al. Bone marrow fibroblasts parallel multiple myeloma progression in patients and mice: in vitro and in vivo studies. Leukemia 2014;28:904–16.
10. Ribatti D, Mangialardi G, Vacca A. Antiangiogenic therapeutic approaches in multiple myeloma. Curr Cancer Drug Targets 2012;12:768–75.
11. Bianco M, Gasparri AM, Colombo B, Curnis F, Girlanda S, Ponzoni M, et al. Chromogranin a is preferentially cleaved into proangiogenic peptides in the bone marrow of multiple myeloma patients. Cancer Res 2016;76:1781–91.
12. Kocemba KA, van Andel H, de Haan-Kramer A, Mahtouk K, Versteeg R, Kersten MJ, et al. The hypoxia target adrenomedullin is aberrantly expressed in multiple myeloma and promotes angiogenesis. Leukemia 2013;27:1729–37.
13. Ria R, Roccaro AM, Merchionne F, Vacca A, Dammacco F, Ribatti D. Vascular endothelial growth factor and its receptors in multiple myeloma. Leukemia 2003;17:1961–6.
14. Moschetta M, Mishima Y, Kawano Y, Manier S, Paiva B, Palomera L, et al. Targeting vasculogenesis to prevent progression in multiple myeloma. Leukemia 2016;30:1103–15.
15. Azab AK, Sahin I, Moschetta M, Mishima Y, Burwick N, Zimmermann J, et al. CXCR7-dependent angiogenic mononuclear cell trafficking regulates tumor progression in multiple myeloma. Blood 2014;124:1905–14.
16. Quach H, Ritchie D, Stewart AK, Neeson P, Harrison S, Smyth MJ, et al. Mechanism of action of immunomodulatory drugs (IMiDS) in multiple myeloma. Leukemia 2010;24:22–32.
17. Kania A, Klein R. Mechanisms of ephrin-Eph signalling in development, physiology and disease. Nat Rev Mol Cell Biol 2016;17:240–56.
18. Wang HU, Chen ZF, Anderson DJ. Molecular distinction and angiogenic interaction between embryonic arteries and veins revealed by ephrin-B2 and its receptor Eph-B4. Cell 1998;93:741–53.
19. Adams RH, Wilkinson GA, Weiss C, Diella F, Gale NW, Deutsch U, et al. Roles of ephrinB ligands and EphB receptors in cardiovascular development: demarcation of arterial/venous domains, vascular morphogenesis, and sprouting angiogenesis. Genes Dev 1999;13:295–306.
20. Robichaux MA, Chenaux G, Ho HY, Soskis MJ, Dravis C, Kwan KY, et al. EphB receptor forward signaling regulates area-specific reciprocal thalamic and cortical axon pathfinding. Proc Nat Acad Sci USA 2014;111:2188–93.
21. Lim BK, Matsuda N, Poo MM. Ephrin-B reverse signaling promotes structural and functional synaptic maturation in vivo. Nat Neurosci 2008;11:160–9.
22. Lu Q, Sun EE, Klein RS, Flanagan JG. Ephrin-B reverse signaling is mediated by a novel PDZ-RGS protein and selectively inhibits G protein-coupled chemoattraction. Cell 2001;105:69–79.
23. Bartolome A, Suda N, Yu J, Zhu C, Son J, Ding H, et al. Notch-mediated Ephrin signaling disrupts islet architecture and beta cell function. JCI Insight 2022;7:e157694.
24. Sawamiphak S, Seidel S, Essmann CL, Wilkinson GA, Pitulescu ME, Acker T, et al. Ephrin-B2 regulates VEGFR2 function in developmental and tumour angiogenesis. Nature 2010;465:487–91.
25. Kwak H, Salvucci O, Weigert R, Martinez-Torrecuadrada JL, Henkemeyer M, Poulos MG, et al. Sinusoidal ephrin receptor EPHB4 controls hematopoietic progenitor cell mobilization from bone marrow. J Clin Invest 2016;126:4554–68.
26. Kou CJ, Kandpal RP. Differential expression patterns of eph receptors and ephrin ligands in human cancers. Biomed Res Int 2018;2018:7390104.
27. Kinch MS, Moore MB, Harpole DH Jr. Predictive value of the EphA2 receptor tyrosine kinase in lung cancer recurrence and survival. Clin Cancer Res 2003;9:613–8.

28. Amato KR, Wang S, Tan L, Hastings AK, Song W, Lovly CM, et al. EPHA2 blockade overcomes acquired resistance to EGFR kinase inhibitors in lung cancer. Cancer Res 2016;76:305–18.
29. Zelinski DP, Zantek ND, Stewart JC, Irizarry AR, Kinch MS. EphA2 overexpression causes tumorigenesis of mammary epithelial cells. Cancer Res 2001;61:2301–6.
30. Zhuang G, Brantley-Sieders DM, Vaught D, Yu J, Xie L, Wells S, et al. Elevation of receptor tyrosine kinase EphA2 mediates resistance to trastuzumab therapy. Cancer Res 2010;70:299–308.
31. Oweida A, Bhatia S, Hirsch K, Calame D, Griego A, Keysar S, et al. Ephrin-B2 overexpression predicts for poor prognosis and response to therapy in solid tumors. Mol Carcinog 2017;56:1189–96.
32. Sandler VM, Lis R, Liu Y, Kedem A, James D, Elemento O, et al. Reprogramming human endothelial cells to haematopoietic cells requires vascular induction. Nature 2014;511:312–8.
33. Noren NK, Lu M, Freeman AL, Koolpe M, Pasquale EB. Interplay between EphB4 on tumor cells and vascular ephrin-B2 regulates tumor growth. Proc Nat Acad Sci USA 2004;101:5583–8.
34. Frigyesi I, Adolfsson J, Ali M, Christophersen MK, Johnsson E, Turesson I, et al. Robust isolation of malignant plasma cells in multiple myeloma. Blood 2014;123:1336–40.
35. Dobin A, Davis CA, Schlesinger F, Drenkow J, Zaleski C, Jha S, et al. STAR: ultrafast universal RNA-seq aligner. Bioinformatics 2013;29:15–21.
36. Kramer A, Green J, Pollard J Jr, Tugendreich S. Causal analysis approaches in ingenuity pathway analysis. Bioinformatics 2014;30:523–30.
37. Zhan F, Huang Y, Colla S, Stewart JP, Hanamura I, Gupta S, et al. The molecular classification of multiple myeloma. Blood 2006;108:2020–8.
38. Barwick BG, Gupta VA, Matulis SM, Patton JC, Powell DR, Gu Y, et al. Chromatin accessibility identifies regulatory elements predictive of gene expression and disease outcome in multiple myeloma. Clin Cancer Res 2021;27:3178–89.
39. Barwick BG, Neri P, Bahlis NJ, Nooka AK, Dhodapkar MV, Jaye DL, et al. Multiple myeloma immunoglobulin lambda translocations portend poor prognosis. Nat Commun 2019;10:1911.
40. Matsui W, Huff CA, Wang Q, Malehorn MT, Barber J, Tanhehco Y, et al. Characterization of clonogenic multiple myeloma cells. Blood 2004;103:2332–6.
41. McMillin DW, Delmore J, Weisberg E, Negri JM, Geer DC, Klippel S, et al. Tumor cell-specific bioluminescence platform to identify stroma-induced changes to anticancer drug activity. Nat Med 2010;16:483–9.
42. Chesi M, Robbiani DF, Sebag M, Chng WJ, Affer M, Tiedemann R, et al. AID-dependent activation of a MYC transgene induces multiple myeloma in a conditional mouse model of post-germinal center malignancies. Cancer Cell 2008;13:167–80.
43. Chesi M, Matthews GM, Garbitt VM, Palmer SE, Shortt J, Lefebure M, et al. Drug response in a genetically engineered mouse model of multiple myeloma is predictive of clinical efficacy. Blood 2012;120:376–85.
44. Pasquale EB. Eph receptors and ephrins in cancer: bidirectional signalling and beyond. Nat Rev Cancer 2010;10:165–80.
45. Arvanitis D, Davy A. Eph/ephrin signaling: networks. Genes Dev 2008;22:416–29.
46. Abengozar MA, de Frutos S, Ferreiro S, Soriano J, Perez-Martinez M, Olmeda D, et al. Blocking ephrinB2 with highly specific antibodies inhibits angiogenesis, lymphangiogenesis, and tumor growth. Blood 2012;119:4565–76.
47. Bong YS, Lee HS, Carim-Todd L, Mood K, Nishanian TG, Tessarollo L, et al. ephrinB1 signals from the cell surface to the nucleus by recruitment of STAT3. Proc Nat Acad Sci U S A 2007;104:17305–10.
48. Salvucci O, Ohnuki H, Maric D, Hou X, Li X, Yoon SO, et al. EphrinB2 controls vessel pruning through STAT1-JNK3 signalling. Nat Commun 2015;6:6576.
49. Bhatia S, Nguyen D, Darragh LB, Van Court B, Sharma J, Knitz MW, et al. EphB4 and ephrinB2 act in opposition in the head and neck tumor microenvironment. Nat Commun 2022;13:3535.
50. Su SA, Yang D, Wu Y, Xie Y, Zhu W, Cai Z, et al. EphrinB2 regulates cardiac fibrosis through modulating the interaction of Stat3 and TGF-beta/Smad3 signaling. Circ Res 2017;121:617–27.
51. Bharti AC, Shishodia S, Reuben JM, Weber D, Alexanian R, Raj-Vadhan S, et al. Nuclear factor-kappaB and STAT3 are constitutively active in CD138+ cells derived from multiple myeloma patients, and suppression of these transcription factors leads to apoptosis. Blood 2004;103:3175–84.
52. Chim CS, Fung TK, Cheung WC, Liang R, Kwong YL. SOCS1 and SHP1 hypermethylation in multiple myeloma: implications for epigenetic activation of the Jak/STAT pathway. Blood 2004;103:4630–5.
53. Li J, Favata M, Kelley JA, Caulder E, Thomas B, Wen X, et al. INCB16562, a JAK1/2 selective inhibitor, is efficacious against multiple myeloma cells and reverses the protective effects of cytokine and stromal cell support. Neoplasia 2010;12:28–38.
54. Scuto A, Krejci P, Popplewell L, Wu J, Wang Y, Kujawski M, et al. The novel JAK inhibitor AZD1480 blocks STAT3 and FGFR3 signaling, resulting in suppression of human myeloma cell growth and survival. Leukemia 2011;25:538–50.
55. Monaghan KA, Khong T, Burns CJ, Spencer A. The novel JAK inhibitor CYT387 suppresses multiple signalling pathways, prevents proliferation and induces apoptosis in phenotypically diverse myeloma cells. Leukemia 2011;25:1891–9.
56. Chavez A, Scheiman J, Vora S, Pruitt BW, Tuttle M, Iyer EPR, et al. Highly efficient Cas9-mediated transcriptional programming. Nat Methods 2015;12:326–8.
57. Darling TK, Lamb TJ. Emerging roles for eph receptors and ephrin ligands in immunity. Front Immunol 2019;10:1473.
58. Dravis C, Yokoyama N, Chumley MJ, Cowan CA, Silvany RE, Shay J, et al. Bidirectional signaling mediated by ephrin-B2 and EphB2 controls urorectal development. Dev Biol 2004;271:272–90.
59. Xu NJ, Henkemeyer M. Ephrin-B3 reverse signaling through Grb4 and cytoskeletal regulators mediates axon pruning. Nat Neurosci 2009;12:268–76.
60. Cowan CA, Henkemeyer M. The SH2/SH3 adaptor Grb4 transduces B-ephrin reverse signals. Nature 2001;413:174–9.
61. Giorgio C, Zanotti I, Lodola A, Tognolini M. Ephrin or not? Six tough questions on Eph targeting. Expert Opin Ther Targets 2020;24:403–15.
62. Dai D, Huang Q, Nussinov R, Ma B. Promiscuous and specific recognition among ephrins and Eph receptors. Biochim Biophys Acta 2014;1844:1729–40.
63. Meyer S, Hafner C, Guba M, Flegel S, Geissler EK, Becker B, et al. Ephrin-B2 overexpression enhances integrin-mediated ECM-attachment and migration of B16 melanoma cells. Int J Oncol 2005;27:1197–206.
64. Nakada M, Drake KL, Nakada S, Niska JA, Berens ME. Ephrin-B3 ligand promotes glioma invasion through activation of Rac1. Cancer Res 2006;66:8492–500.
65. Pennisi A, Ling W, Li X, Khan S, Shaughnessy JD Jr., Barlogie B, et al. The ephrinB2/EphB4 axis is dysregulated in osteoprogenitors from myeloma patients and its activation affects myeloma bone disease and tumor growth. Blood 2009;114:1803–12.
66. Caivano A, La Rocca F, Laurenzana I, Annese T, Tamma R, Famigliari U, et al. Epha3 acts as proangiogenic factor in multiple myeloma. Oncotarget 2017;8:34298–309.
67. La Rocca F, Airoldi I, Di Carlo E, Marotta P, Falco G, Simeon V, et al. EphA3 targeting reduces in vitro adhesion and invasion and in vivo growth and angiogenesis of multiple myeloma cells. Cell Oncol (Dordr) 2017;40:483–96.
68. Ding L, Shen Y, Ni J, Ou Y, Ou Y, Liu H. EphA4 promotes cell proliferation and cell adhesion-mediated drug resistance via the AKT pathway in multiple myeloma. Tumour Biol 2017;39:1010428317694298.
69. Alam SK, Yadav VK, Bajaj S, Datta A, Dutta SK, Bhattacharyya M, et al. DNA damage-induced ephrin-B2 reverse signaling promotes chemoresistance and drives EMT in colorectal carcinoma harboring mutant p53. Cell Death Differ 2016;23:707–22.
70. Sasabe E, Tomomura A, Tomita R, Sento S, Kitamura N, Yamamoto T. Ephrin-B2 reverse signaling regulates progression and lymph node metastasis of oral squamous cell carcinoma. PLoS One 2017;12:e0188965.
71. Nakada M, Anderson EM, Demuth T, Nakada S, Reavie LB, Drake KL, et al. The phosphorylation of ephrin-B2 ligand promotes glioma cell migration and invasion. Int J Cancer 2010;126:1155–65.
72. Takeuchi S, Katoh H, Negishi M. Eph/ephrin reverse signalling induces axonal retraction through RhoA/ROCK pathway. J Biochem 2015;158:245–52.
73. Salvucci O, de la Luz Sierra M, Martina JA, McCormick PJ, Tosato G. EphB2 and EphB4 receptors forward signaling promotes SDF-1-induced endothelial cell chemotaxis and branching remodeling. Blood 2006;108:2914–22.
74. Martiny-Baron G, Holzer P, Billy E, Schnell C, Brueggen J, Ferretti M, et al. The small molecule specific EphB4 kinase inhibitor NVP-BHG712 inhibits VEGF driven angiogenesis. Angiogenesis 2010;13:259–67.
75. Kertesz N, Krasnoperov V, Reddy R, Leshanski L, Kumar SR, Zozulya S, et al. The soluble extracellular domain of EphB4 (sEphB4) antagonizes EphB4-EphrinB2 interaction, modulates angiogenesis, and inhibits tumor growth. Blood 2006;107:2330–8.